Neurobiology of Disease 194 (2024) 106463

Contents lists available at ScienceDirect

Neurobiology of Disease

journal homepage: www.elsevier.com/locate/ynbdi

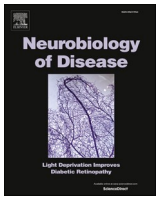

Specific photoreceptor cell fate pathways are differentially altered in NR2E3-associated diseases

Izarbe Aísa-Marín [a,b,c,1], Quirze Rovira [d,1], Noelia Díaz [d,2], Laura Calvo-López [a], Juan M. Vaquerizas [d,e,f,*], Gemma Marfany [a,b,c,g,*]

[a] Department de Genètica, Microbiologia i Estadística, Universitat de Barcelona, Barcelona 08028, Spain
[b] IBUB-IRSJD, Institut de Biomedicina de la Universitat de Barcelona-Institut de Recerca Sant Joan de Déu, Barcelona 08028, Spain
[c] CIBERER, Instituto de Salud Carlos III, Barcelona 08028, Spain
[d] Max-Planck-Institute for Molecular Biomedicine, Münster 48149, Germany
[e] MRC London Institute of Medical Sciences, Institute of Clinical Sciences, Imperial College London, London W12 0NN, UK.
[f] Institute of Clinical Sciences, Faculty of Medicine, Imperial College London, Du Cane Road, London W12 0NN, UK
[g] DBGen Ocular Genomics, Barcelona 08028, Spain

ARTICLE INFO

Keywords:
Inherited retinal dystrophies
NR2E3
Photoreceptor differentiation
Retinal development
Single-cell RNA-seq

ABSTRACT

Mutations in *NR2E3,* a gene encoding an orphan nuclear transcription factor, cause two retinal dystrophies with a distinct phenotype, but the precise role of NR2E3 in rod and cone transcriptional networks remains unclear. To dissect NR2E3 function, we performed scRNA-seq in the retinas of wildtype and two different *Nr2e3* mouse models that show phenotypes similar to patients carrying *NR2E3* mutations. Our results reveal that rod and cone populations are not homogeneous and can be separated into different sub-classes. We identify a previously unreported cone pathway that generates hybrid cones co-expressing both cone- and rod-related genes. In mutant retinas, this hybrid cone subpopulation is more abundant and includes a subpopulation of rods transitioning towards a cone cell fate. Hybrid photoreceptors with high misexpression of cone- and rod-related genes are prone to regulated necrosis. Overall, our results shed light on the role of NR2E3 in modulating photoreceptor differentiation towards cone and rod fates and explain how different mutations in *NR2E3* lead to distinct visual disorders in humans.

1. Introduction

The retina is the light-sensitive tissue responsible for visual perception. Retinal photoreceptors are specialized neurons that detect light photons and initiate the signal transduction from the retina to the brain. Human retina photoreceptors include rods –responsive to dim light conditions– and three types of cones expressing opsins sensitive to short, medium and long wavelength light (S-, M- and L-cones, respectively), which mediate colour vision and visual acuity (Nathans et al., 1986; Schnapf et al., 1987). Instead, the mouse retina is formed by rods and cones that express S- and M-opsins. A careful orchestration of regulatory transcription factors is thus required to determine photoreceptor fate and differentiation during retinal development.

In the developing mouse retina, differentiation into S-cones is the default fate path for photoreceptor precursor cells (PPCs) unless additional regulatory signals determine them towards rod or M-cone identities (Swaroop et al., 2010). In this process, the retinal transcription factor NRL acts upstream of NR2E3, the latter displaying a dual function as both transcriptional activator and repressor in photoreceptors. NR2E3 is an orphan nuclear receptor that can homodimerize and form a

Abbreviations: AF2, activation-function-2 helix; Cry, crystallin; CSTB, Cathepsin B; DE, differential expressed; ESCS, enhanced S-cone syndrome; GFS, Goldmann-Favre syndrome; GO, gene ontology; H10, helix 10 domain; IRD, inherited retinal dystrophy; MLKL, Mixed lineage kinase domain like pseudokinase; NR2E3, Nuclear receptor subfamily 2 group E member 3; NRL, Neural retina leucine zipper; OXPHOS, oxidative phosphorylation; PARP-1, poly(ADP-ribose) polymerase 1; PPCs, photoreceptor precursor cells; RP, retinitis pigmentosa; RPCs, retinal progenitor cells; RPE, retinal pigment epithelium cells; scRNA-seq, single-cell RNA-sequencing; SD, standard deviation; VDAC, Voltage-dependent anion-selective channel; wt, wildtype.

* Corresponding authors.
E-mail addresses: j.vaquerizas@lms.mrc.ac.uk (J.M. Vaquerizas), gmarfany@ub.edu (G. Marfany).
[1] These authors contributed equally to this work.
[2] Current address: Institute of Marine Sciences, The Spanish National Research Council (CSIC), 08003, Spain.

https://doi.org/10.1016/j.nbd.2024.106463
Received 27 December 2023; Received in revised form 1 March 2024; Accepted 2 March 2024
Available online 12 March 2024

transcription regulatory complex together with CRX and NRL to repress the cone-default pathway and activate the expression of rod-specific genes (Chen et al., 2005; Cheng et al., 2006; Peng et al., 2005). In the mature retina, NR2E3 is also necessary for rod homeostasis and maintenance (Cheng et al., 2004; Haider, 2001).

Analysis of the NR2E3 crystal structure revealed an auto-repressed conformation, with the formation of an homodimer, mainly directed by the helix 10 domain (H10), where the activation-function-2 helix (AF2) is allocated into the canonical cofactor binding site in the homodimer (Tan et al., 2013). Therefore, both the AF2 domain and dimerization are both required for NR2E3 role as a transcriptional repressor, and the switch towards activation would require binding to other cofactors (Kanda and Swaroop, 2009; Tan et al., 2013). Two transcript isoforms of NR2E3 have been identified in both humans and mouse (Aísa-Marín et al., 2020a). The long isoform spans 8 exons and produces the conventional NR2E3 protein (410 aa and 395 aa, in human and mouse, respectively), whereas the shorter transcript isoform retains intron 7 and thus generates a shorter protein that lacks exon 8 (367 aa in human (computational prediction) and 352 aa in mouse). Since exon 8 encodes the H10 and AF2 helices, the shorter NR2E3 protein isoform (which is developmentally regulated in mouse) cannot dimerize nor act as a repressor, and its physiological function remains to be elucidated.

Diseases associated with *NR2E3* include retinitis pigmentosa (RP, MIM# 611131) and enhanced S-cone syndrome (ESCS; MIM# 268100), whose most severe affectation is also named as Goldmann-Favre syndrome (GFS; MIM# 26800)(Bernal et al., 2008; Coppieters et al., 2007; Gire et al., 2007; Haider et al., 2000; Schorderet and Escher, 2009). Some *NR2E3* mutations affect rod maintenance and survival in the mature retina and cause RP, a neurodegenerative retinal dystrophy characterized by progressive loss of rod photoreceptors followed later by cones. RP is caused by mutations inherited following mostly an autosomal dominant (Schorderet and Escher, 2009) –but in a few cases autosomal recessive (Gerber et al., 2000; Kannabiran et al., 2012); –(Bocquet et al., 2013) pattern. On the other hand, most reported mutations affect the inhibition of the cone pathway and result in autosomal recessive ESCS, characterized by an excess of dysfunctional S-cones in detriment of rods. *NR2E3* mutations are scattered throughout the whole gene and there is scarce knowledge on the molecular mechanisms leading to the distinct clinical phenotypes (Schorderet and Escher, 2009).

We previously generated two *Nr2e3* mouse models using CRISPR-Cas9 editing to delete different domains encoded in the last exon (Aísa-Marín et al., 2020b, 2020a). The *Nr2e3* Δ27 model –carrying a homozygous in-frame deletion that ablates the H10 domain– shows an ESCS-like phenotype, with profound but non-progressive alterations in retinal function (Aísa-Marín et al., 2020a). The *Nr2e3* ΔE8 model –carrying a complete deletion of exon 8 so that only the short isoform is expressed– shows a RP-like phenotype that progressively leads to neurodegeneration (Aísa-Marín et al., 2020a). Notably, both mutants present cone-rich invaginations in the central retina, similar to the rosettes observed in the *rd7* mouse retina, a natural model of ESCS caused by a LINE transposon insertion that disrupts the *Nr2e3* gene (Akhmedov et al., 2000; Chen et al., 2006; Haider, 2001).

In addition to histological characterization, retinal transcriptomic analyses through bulk RNA-seq have been widely used to identify the molecular mechanisms underlying pathological processes that cause retinal dystrophies (Bales et al., 2018; Liu et al., 2020; Uren et al., 2014). However, subtle transcriptomic differences between differentiated photoreceptors might go undetected, which is critical when studying the NR2E3 opposing roles in rod and cone transcriptional networks. Here we present single-cell RNA-seq results on these two *Nr2e3* models retinas by comparing the distinct cell types and photoreceptor sub-populations that make up the wildtype (wt) and *Nr2e3* mutant retinas.

Our results unveil different and undescribed sub-populations within cone and rod cell populations, highlight gene expression changes in rod and cone cells and detect photoreceptor cells with a hybrid rod-cone expression pattern in the *Nr2e3* mutants, all in agreement with NR2E3 dual function as transcriptional activator of rod genes and repressor of cone genes.

2. Materialandmethods

2.1. Resource availability, lead contact

For mouse and reagent requests, contact Gemma Marfany (gmarfany@ub.edu).

2.2. Resource availability, data and code availability

Raw single-cell RNA-seq data have been deposited at ArrayExpress (accession E-MTAB-12183) and are publicly available as of the date of publication. Accession numbers are listed in the resources table. Requests on scRNA-Seq data and analyses should be directed to Juanma Vaquerizas (j.vaquerizas@lms.mrc.ac.uk).

2.3. Animals and ethical statement

Nr2e3 wt, Δ27 and ΔE8 mice (C57BL7/6 J background) were used in all experiments described in the article. In all assays and per genotype, both biological sexes were used in equivalent numbers, and age-matched between P40-P80 (young animals, <3 months old, unless otherwise stated). Animal handling, euthanasia and surgical dissections were performed according to the ARVO statement for the use of animals in ophthalmic and vision research, following the animal care guidelines of the University of Barcelona and with the approval of the Ethics Committee for animal experimentation File number FUE-2019-00965313, ID 2MDLDY4WZ, and the Bioethics Committee.

2.4. Single-cell dissociation, methanol fixation, rehydration and cDNA library preparation

Two retinas per animal (three wild-type and two per each mutant) were used, including in each genotype at least one male and one female, and with closely related age matches between P40-P80 (WT.1 - P80 male; WT.2 - P40 female; WT.3 - P40 female; Δ27.1 - P80 male; Δ27.2 - P80 female; ΔE8.1 - P40 female; ΔE8.2 —P40 male). Retinas were dissected the same day and hour (1 h–2 h after light exposure in the day/night cycle at the animal facility) in Neurobasal media and placed on ice, transferred to a papain solution (Neural Tissue Dissociation Kit – Postnatal Neurons, Milteny Biotec) and incubated at 37 °C for 15 min (agitation at 5-min intervals), following the manufacturer's instructions. DNase I (10 U/ml, Roche) was added and incubated at 37 °C for additional 5 min. Samples were homogenized by gently pipetting, and cells were centrifuged at 400*g* for 5 min at 4 °C. Methanol fixation and rehydration were performed according to the Single Cell RNA Sequencing guidelines of 10× Genomics. Briefly, a minimum of 1×10^6 cells were resuspended in 200 ml of cold PBS and 800 ml of cold methanol. Cell suspension was placed on ice for 30 min prior to transferring to −80 °C for long-term storage (up to 6 weeks). For rehydration, cells were placed on ice for 5 min, centrifuged at 1000*g* for 5 min at 4 °C and resuspended in 300 ml of Wash Resuspension Buffer (0.04% BSA, 1 mM DTT, 0.2 U/ml Rnase inhibitor in 3× SSC buffer). The cell suspension was filtered through a 50-μm cell strainer. Processing for single-cell capture and library preparation followed the 10× Genomics standard protocols.

2.5. Immunostaining of mouse retinal sections

The dissection of retinas and eyecups from wt and mutant mice was performed as previously described (Toulis et al., 2016). Cryosections of mouse retinas (10–12 μm slides, obtained with a Leica CM3050-S cryostat) were immunostained as reported elsewhere (Aísa-Marín

et al., 2020a). Working dilutions for the antibodies were as follows: anti-GNAT2 (Abcam ab97501, 1:300), anti-RHO (Abcam ab5417, 1:300), anti-CRYBB2 (Santa Cruz sc-376,006, 1:200), anti-S-OPSIN (Millipore AB5407, 1:300), anti-M-OPSIN (Millipore AB5405, 1:300), anti-CTSB (Abcam ab58802, 1:200), anti-MLKL 9hosphor S358 (Abcam ab187091, 1:200), anti-PAR (Abcam ab14459, 1:200). The specificity of each antibody was assessed by introducing a negative control, wherein only the secondary antibody was used, and by comparing the staining of the protein of interest as reported in previous work from ours or other groups. Slides were mounted using ProLong™ Gold Antifade Mountant (Thermo Fisher Scientific), and kept refrigerated until confocal microscopy (Carl Zeiss LSM880). For CTSB quantification, images obtained with the confocal microscope (Carl Zeiss LSM880) were analysed using the Image J image processing software (Rasband, W.S., ImageJ, U. S. National Institutes of Health, Bethesda, Maryland, USA).

2.6. Electrophoresis of proteins in polyacrylamide gels (SDS-PAGE), Western blot and immunodetection

Retinal protein lysates of each genotype (see details in the Animal subsection) were obtained in radioimmunoprecipitation assay (RIPA) buffer, electrophoresed and transferred to a PVDF Western Blotting Membrane (Bio Rad) as previously reported (Aísa-Marín et al., 2020a). The membrane was blocked with 10% non-fat dry milk in PBS containing 0.1% Tween 20 (Sigma-Aldrich). Primary antibodies (anti-GNAT2 [Abcam ab97501, 1:1000], anti-CRYAA [Abcam ab5595, 1:1000], anti-VDAC [Calbiochem Ab-5185–197, 1:7000], and rodent total OXPHOS cocktail [MitoSciences 6 μg/ml]) were incubated overnight at 4 °C, followed by a secondary antibody incubation for 1 h at room temperature. Proteins were visualized using the Luminescent Image Analyzer LAS-3000 mini (Fujifilm, Tokyo, Japan).

2.7. RNA isolation and reverse transcriptase PCR (RT-PCR)

Mouse retinas were homogenized using a Polytron PT1200E homogenizer (Kinematica, AG, Lucerne, Switzerland). Total RNA was isolated using the Rneasy Mini Kit (Qiagen, Germantown, MD) and Rneasy Plus Mini Kit (Qiagen, Germantown, MD), following the manufacturer's instructions with minor modifications (treatment with DNAse I during 1 h). Reverse transcription reactions were carried out using the qScriptTM cDNA Synthesis Kit (Quanta BioSciences, Inc., Gaithersburg, MD). Specific primers for amplification were designed and optimized. RT-PCR was performed according to standard thermocycling conditions.

2.8. Primary retinal cell cultures

Primary retinal cells were cultured after dissecting P0–1 mouse retinas and processed as reported (Mirra et al., 2021). Briefly, the cell suspension was obtained using Neural Tissue Dissociation Kit (Miltenyi Biotec, Germany), and 150,000 cells were plated onto poly-D-ornithine-laminin-coated coverslips in Neurobasal™-A medium (Thermo Fisher Scientific) supplemented with 0.06% glucose, 0.0045% NaH2CO3,1 mM L-glutamine, B27 (Invitrogen), penicillin/streptomycin (Invitrogen 1%), forskolin 5 μM (Sigma Aldrich), BDNF 5 ng/ml (Peprotech) and rat CNTF 20 ng/ml (Peprotech). After 7 days of differentiation in vitro (7DIV), cells were fixed and stored in cryoprotection buffer (30% Glycerol, 25% Etilenglicol 100% and 0.1 M PBS.

2.9. Single-cell RNA-seq analysis

2.9.1. Pre-processing

Raw reads were trimmed with fastp (version 0.20.0) (Chen et al., 2018). 10× Genomics Cell Ranger (version 6.0.1) (Zheng et al., 2017) was used for barcode processing, mouse reference genome alignment (GENCODE vM23/Ensembl 98; https://support.10xgenomics.com/single-cell-gene-expression/software/downloads/latest?), and feature-barcode matrices generation. Cells were filtered by the number of counts and feature numbers to remove the top and bottom 5% of cells representing outliers (Luecken and Theis, 2019). Doublets were found and filtered using DoubletFinder (version 2.0.3) (McGinnis et al., 2019). Initial data examination revealed a broad presence of rod-cell marker expression throughout all individual cells, which was attributed to ambient RNA contamination from this abundant and morphologically challenging cell population. SoupX (version 1.5.2) (Young and Behjati, 2020) was used prior to cell filtering to remove ambient RNA using the functions autoEstCont(sc,forceAccept = TRUE) and adjustCounts(sc). After cleaning ambient RNA, expression of specific gene markers (e.g. *Nrl* and *Rho* for rods) was highly enriched in the corresponding retinal cell population as shown in UMAP plots (Fig. 1). Data is available at Suppl. Data 1.

2.9.2. Integration and clustering

The R package Seurat (version 4.1.0) (Butler et al., 2018; Stuart et al., 2019) was used to integrate our samples with a publicly available mouse retina scRNA-seq dataset (Norrie et al., 2019). The use of a trusted reference to integrate our data ensured better cell clustering identity and downstream analysis robustness of our scRNA-seq data. Sample integration was performed using the SCT normalization method. SCT transformed data were clustered using the first 30 principal components (PCs) and a resolution of 0.25.

2.9.3. Cell type identification and differential expression

RNA assay from the Seurat object was normalized and scaled to detect cell type markers. A set of variable features was identified using selection.method = "vst". The FindAllMarkers function was then used to detect cluster-specific markers. Cluster cell identity was manually determined using known cell type markers (Hoang et al., 2020). Annotated Seurat clusters confidently sharing cell type markers were joined for downstream analysis. Misregulated genes for each cell type between wt samples and mutants were identified using the FindMarkers function. Resulting *p*-values were adjusted for multiple testing using p.adjust (method = "fdr") as implemented in R (version 4.0.1).

2.9.4. Cone and rod sub-clustering

Cells identified as cone or rod were subset separately and re-clustered using SCT transformed data taking the first 20 PCs and a resolution of 0.01. Cell type sub-cluster markers were identified using RNA assay and FindAllMarkers as implemented in Seurat. Data is available in Suppl. Data 2 and Suppl. Data 3.

2.9.5. Expression visualization

Violin plots and UMAPs showing gene expression were produced using the counts of the Seurat SCT assay. Violin plots were log-transformed for visual clarity. UMAP expression plots were produced with the Seurat function FeaturePlot with the following arguments: slot = "counts", cols = c("grey","red"), keep.scale = NULL or "feature", order = TRUE, max.cutoff = "q95".

2.9.6. RNA velocity analysis

Unspliced and spliced mRNAs quantification was performed using velocyto (version 0.17.17)(La Manno et al., 2018) with the same reference genome annotation used for Cell Ranger and the mm10 repeat masker annotations downloaded from the UCSC table browser. RNA velocities were calculated using the scVelo (version 3.8.6)(Bergen et al., 2020) package in python (version 3.8.6) in the stochastic mode. To capture genotype specific RNA velocities, those were calculated for wt and mutant samples independently.

2.9.7. Quantification and statistical analysis

Statistical significance of data, equal standard deviation (SD) and normal distribution were first assessed using Bartlett and Shapiro-Wilk tests. If data followed a normal distribution and showed homogeneity

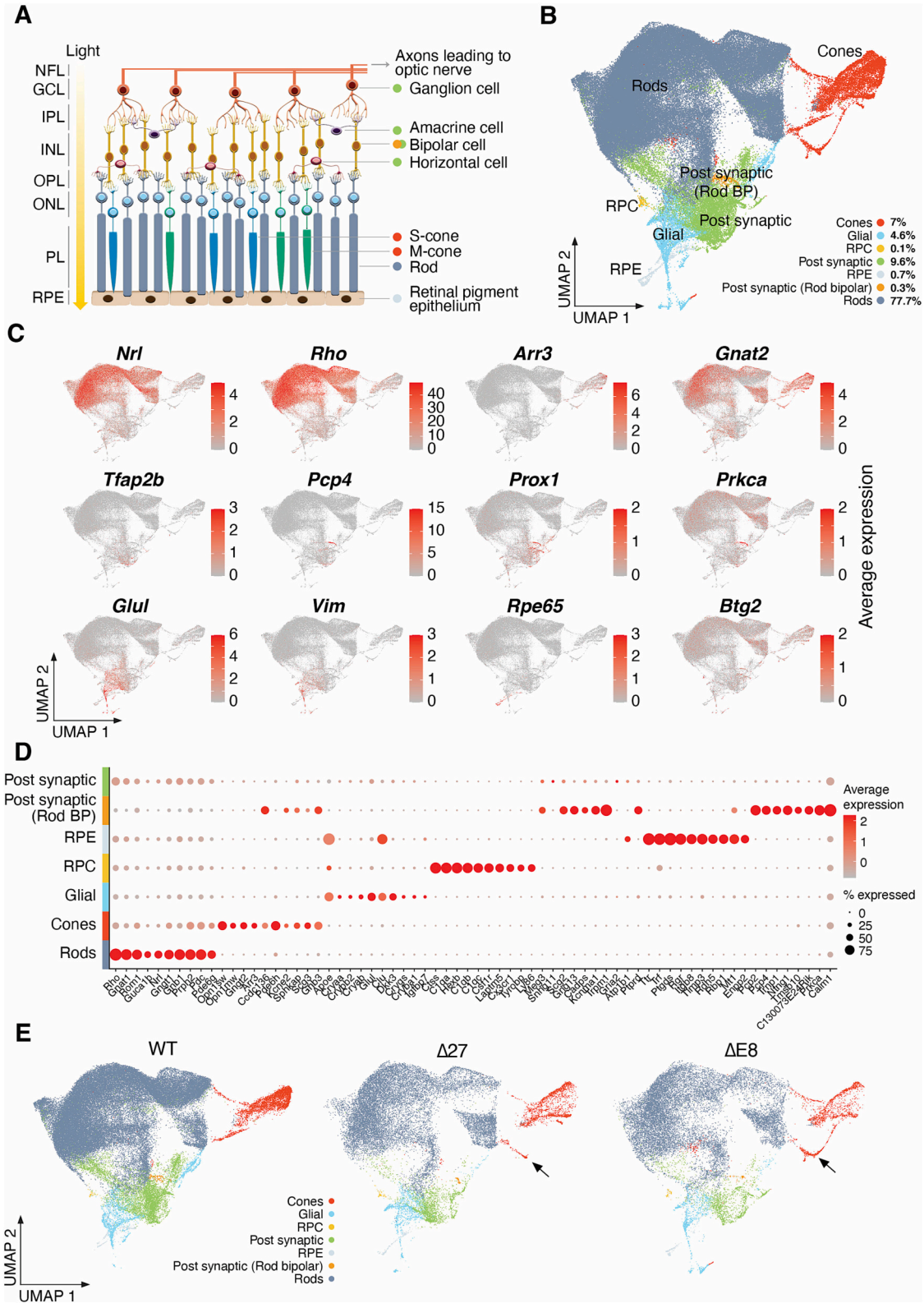

Fig. 1. Single-cell RNA-seq of wildtype and Nr2e3 mutant retinas reveals different cell populations. A. Scheme showing the different functional cell layers and connections within the mouse retina. Colour dots at the right of each cell type name correspond to the cluster assignment in B. B. UMAP plot of sequenced retinal cells showing the clustering of the different cell types. Assignment to main retinal cell types is based on the expression of specific gene markers. C. The expression of signature marker genes across cell groups identifies clusters of rod, cone, post-synaptic, rod bipolar, retinal progenitor cells (RPC), glial and retinal pigment epithelium (RPE) cells. D. Dot plot of signature genes in the different cell types isolated from mouse retinas. E. Differences in the UMAP plot by genotype. Particular subpopulations identified as unique within the cone cluster in the mutant retinas are indicated by a black arrow. See also (Supplementary Fig. 1 and 2).

of variance, one-way ANOVA was used for multiple group statistical significance analysis. When data did not follow a normal distribution, the non-parametrical Kruskal-Wallis test was applied. Analysis was performed using GraphPad Prism 7.03 (San Diego, CA, USA).

3. Results

3.1. Single-cell RNA-seq of wildtype and Nr2e3 mutant retinas reveals different cell populations

We sampled whole retinas from wt and mutant mice at stage P40-P80, a timepoint at which Δ27 and ΔE8 mutant mice have fully developed young adult retinas but phenotypically differ in their electrophysiological recordings (ERGs) (Aísa-Marín et al., 2020a). Thus, Δ27 mutants are visually impaired due to retinal developmental alterations (ESCS-like phenotype), whereas ΔE8 mutants, with a progressive late-onset retinal degeneration still show normal electrophysiological responses (RP-like phenotype) (Aísa-Marín et al., 2020a). Retinal samples were subject to droplet-based single-cell RNA-sequencing (scRNA-seq, 10× Genomics Chromium platform), which resulted in the generation of gene expression libraries for a total of 107,628 cells after quality-control filtering (Supplementary Table 1). To prevent RNA ambient contamination from extremely abundant and fragile rod cells, scRNA-seq data were further filtered using SoupX (Young and Behjati, 2020). Filtered data is provided in Supplementary Data 1.

Next, we used a recent publicly available scRNA-seq dataset of wt mouse retinas (Norrie et al., 2019) to integrate our data for robust clustering and cell-type identification (see Methods). Pooled scRNA-seq data from all retinas were normalized, and we identified seven different retinal cell type clusters, which were assigned based on differential expressed (DE) genes, or signature genes specific to particular cell types (Supplementary Fig. 1) (Fig. 1A-D). High expression levels of *Nrl* and *Rho* identified the rod photoreceptor cluster, and high expression of *Arr3* and *Gnat2* identified the cone cluster (Fig. 1C-1D, Supplementary Fig. 1). Expression of *Tfap2b* and *Prox1* determined horizontal and amacrine cells (Dyer et al., 2003; Jin et al., 2015; Pérez De Sevilla et al., 2017) among the post-synaptic cell cluster, and *Pcp4* determined bipolar (Shekhar et al., 2016) and ganglion cells (Laboissonniere et al., 2019). *Prkca* specifically defined the rod bipolar cell cluster (Ruether et al., 2010; Woods et al., 2018), which was differentiated by the high expression of specific marker genes (Fig. 1D, Supplementary Fig. 1). Expression of *Glul* and *Vim* identified Müller cells (Roesch et al., 2008) and astrocytes (Wunderlich et al., 2015), respectively, in the glial cluster. Finally, high expression levels of *Rpe65* identified a small RPE cell cluster, and *Btg2* was considered a marker of neurogenic RPCs (Trimarchi et al., 2008) (Fig. 1C, Supplementary Fig. 1). These seven major cell type clusters are present in the retinas of all three genotypes (wt, and mutants Δ27 and ΔE8), as detailed in the Supplementary Table 1. Since *Nr2e3* is solely expressed in photoreceptors and we aimed to focus on photoreceptor cell fate, we did not further categorise other retinal cell clusters.

The composition of cell populations across our pooled samples confirmed that the predominant isolated cell were rod photoreceptors (77.7%, Fig. 1B), the primary cell type in the retina of both mice and humans (Jeon et al., 1998). Notably, the retinas of the two mutants display a new subpopulation of cones that clearly stand aside from the rest of the cells in the cone cluster (Fig. 1E, black arrows).

Nr2e3 was expressed in rod and cone photoreceptors of wt and mutant retinas as expected. Visualization of scRNA-seq reads validated the mutation of each *Nr2e3* mutant model and confirmed the 27-nucleotide in-frame deletion and the complete deletion of exon 8 in Δ27 and ΔE8 mutants respectively (Supplementary Fig. 2 A). The scRNA-seq data confirmed the overexpression of *Nr2e3* in the postnatal Δ27 vs wt retinas, and the low *Nr2e3* expression in the ΔE8 mutant (Supplementary Fig. 2B), as previously reported using qRT-PCR (Aísa-Marín et al., 2020a). Nonetheless, in all three genotypes, the *Nr2e3* expression ratio between rods and cones was maintained, being 3 times higher in rods than in cones (Supplementary Fig. 2C).

3.2. Nr2e3 mutant retinas produce hybrid photoreceptors

To identify mutant-specific cell cluster changes in gene expression we analysed the DE genes for the *Nr2e3* mutants compared to the wt samples (Fig. 2A, Supplementary Table 2). Frequent Gene ontology (GO) terms from the DE genes in the rod and cone clusters between the mutant and wt retinas suggest that both cones and rods showed altered gene expression, particularly in genes associated with photoreceptor and neuronal function, but mutant rods show a higher number of DE genes related to neurosensory signalling, phototransduction and photoreception (groups A and B) as well as proteins involved in protein quality control (chaperones, and deubiquitination), autophagy and necrosis pathways (group I) (Fig. 2A, Supplementary Table 2). Consistent with the AF2 domain (required for the repressor function) being either absent (ΔE8) or conformationally inactive (Δ27) in the two mutant NR2E3, most DE genes were overexpressed compared to wt photoreceptors, except with a very clear group of downregulated genes involved in homeostasis, mitochondria, visual longterm conduction and synaptogenesis (Fig. 2A, group G). Opposite alterations in cone versus rod DE can be identified in genes involved in differentiation and eye development, DNA repair mechanisms and translation-associated metabolism (groups C, D and E).

When focusing specifically on the list of retina-specific genes for light perception and transduction, the altered expression in *Nr2e3* mutant photoreceptors becomes very apparent (Supplementary Fig. 3). A relevant subset of rod-specific photoreception and phototransduction genes (e.g. *Gnat1, Gntg1, Rho*) are highly and ectopically expressed in the cones of both mutants (Fig. 2B, Supplementary Fig. 3). Some of these rod-specific genes are also overexpressed in the rods of the mutants (e.g. *Gnat1*, *Gnb1* and *Gngt1*), particularly in the Δ27 samples. In fact, the Δ27 retinas are characterized by a high overexpression of *Nr2e3* in rods, and ectopically, in cones (Fig. 2B, Supplementary Fig. 4). Interestingly, mutant cones express *Gngt1*, a rod transducin associated as a marker of foveal cones that is also overexpressed in S-opsin photoreceptors from *Nrl*-null retinal organoids (Kallman et al., 2020; Peng et al., 2019). Higher levels of *Gngt1* and the foveal marker gene *Cyp26a1* in the mutant retinas was confirmed by RT-PCR in total retina samples (Supplementary Fig. 5).

Moreover, cone-specific genes appear over-expressed because their expression is not correctly repressed. In mutant rods, a subset of genes involved in cone phototransduction (e.g. *Gnat2, Pde6c* and *Pde6h*) are ectopically overexpressed (Fig. 2C, Supplementary Fig. 3 and 4), but this high ectopic misexpression does not affect all cone genes (e.g. *Opn1mw* and *Arr3*). In addition, in mutant cones most cone-specific genes (such as *Gnat2*, *Pde6h*, *Opn1sw*) are also overexpressed, particularly in the Δ27 mutant. Altogether, Δ27 mutant retinas (P40) show a higher number of DE genes than ΔE8 mutants (P80).

To experimentally validate these results, the overexpression of the cone *Gnat2* marker in mutant retinas was analysed by immunohistochemistry and western blot immunodetection. A significant increase of GNAT2 levels (around 20-fold) was detected in the mutant retinas, in agreement with its upregulation in rod and cone photoreceptors (Fig. 2D-E). In the wt retina, GNAT2 expression is restricted to cones in contrast to the mutant retinas, where GNAT2 is misexpressed and localizes in the outer rod segments (Fig. 2F).

Overall, in the *Nr2e3*-mutant retinas, rods ectopically overexpress cone-specific genes, whereas cones ectopically overexpress rod-specific genes, thus unveiling the presence of hybrid photoreceptors, being assigned as hybrid cones or hybrid rods, depending on their clustering into the cone or rod populations.

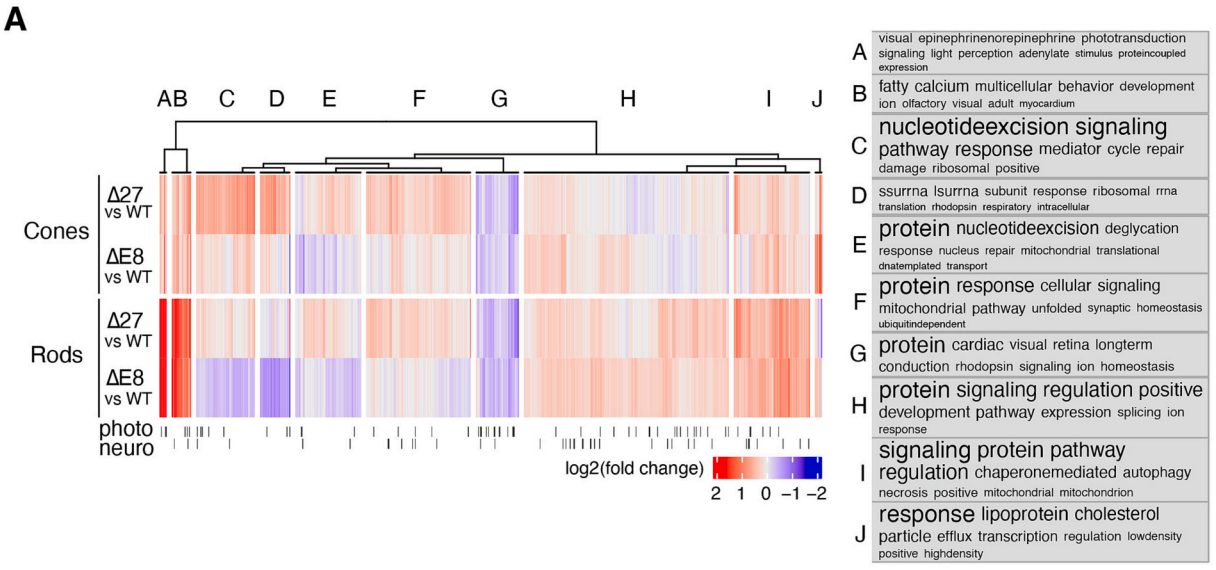

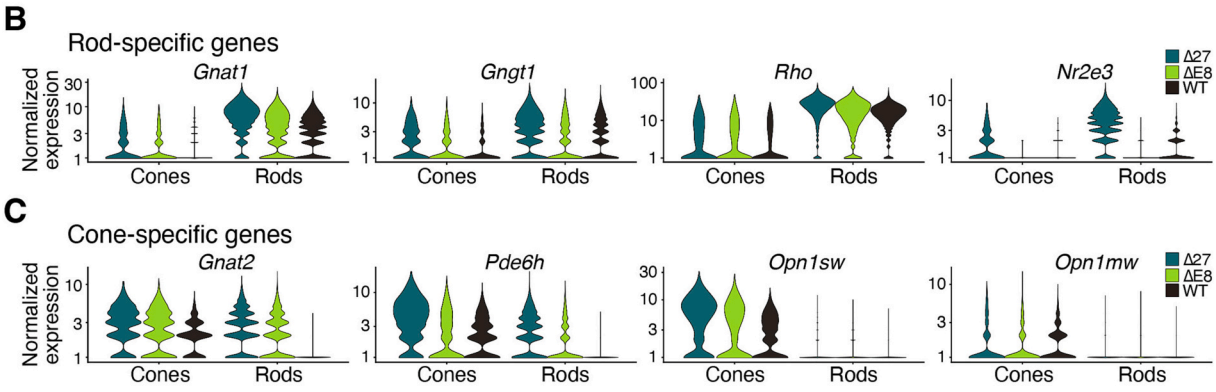

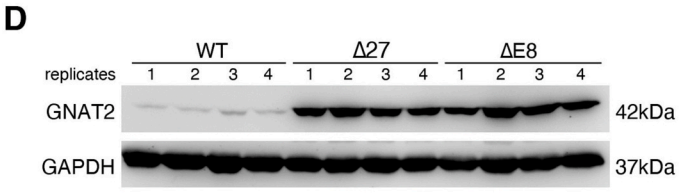

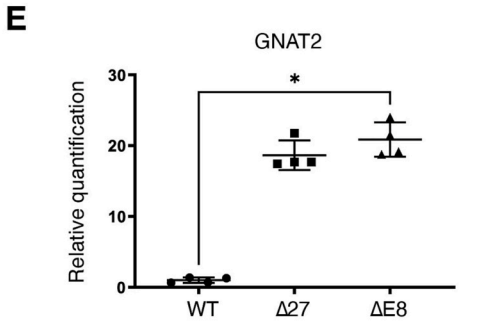

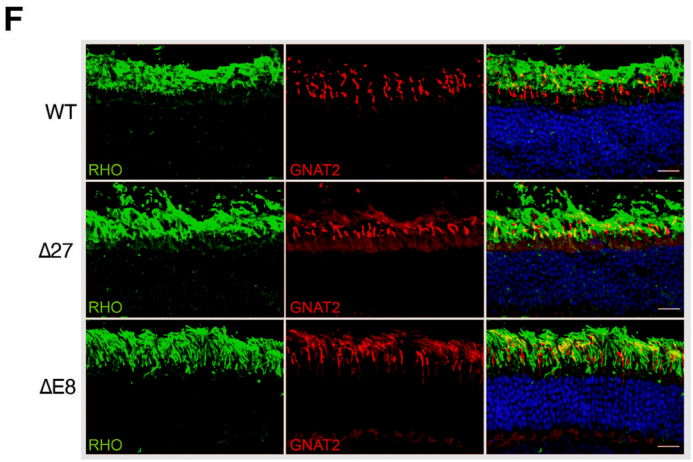

(caption on next page)

Fig. 2. *Nr2e3* mutant retinas produce hybrid photoreceptors. A. Log 2-fold change heatmap showing the DE genes sorted by k-means clustering in the rod and cone clusters of Δ27 and ΔE8 mutants vs wt retinas. Frequent biological process GO terms appear in the cloud according to their association to each cluster. Larger font size indicates higher abundance of the GO term. Photo and Neuro indicate specific photoreceptor and neuronal genes, respectively. B—C. Expression dysregulation of rod- (B) and cone- (C) specific genes in the rod and cone populations from mutant Δ27 and ΔE8 vs wt retinas. Note that some rod genes are overexpressed in cones (e.g., *Gnat1, Gngt1*), whereas cone genes are not repressed in rods (e.g. *Gnat2, Pde6h*). (See the detailed gene list in Supplementary Fig. 3). D—F. Confirmation of the overexpression of GNAT2 (cone-specific) in the wt and mutant retinas (see details of samples in the Material and Methods). D. Western blot immunodetection of *Nr2e3* wt and mutant retinal lysates showing a 20-fold increase of GNAT2 expression in the mutants. Samples 1–12 are independent biological replicates from the three genotypes (1–4 wt, 5–8 Δ27, 9–12 ΔE8). E. Quantification of the data in (D), presented as mean and SD (statistical significance, $*p < 0.02$, Kruskal-Wallis test). F. Immunofluorescence staining of wt and mutant retinas ($n = 3$) shows diffuse localization of GNAT2 (red) in the outer segment of Δ27 and ΔE8 rod photoreceptors (RHO, green). Photoreceptor nuclei are counterstained with DAPI (blue). See also Supplementary Figs. 4 and 5. (For interpretation of the references to colour in this figure legend, the reader is referred to the web version of this article.)

3.3. Distinct cone subpopulations in Nr2e3 mutant retinas suggest alterations in cone photoreceptor fate determination

Interestingly, a careful comparison of the UMAP plot by genotype unveiled that the mutant retinas produce a new subpopulation atypical cone cells that stand aside the rest of cones (Fig. 1E, black arrows). To further investigate these atypical cones, we performed clustering analysis on the cone cell sub-population (Supplementary Data 2) and identified five subclusters (numbered 0 to 4, Fig. 3A). The total number of cones was much lower in the *Nr2e3* mutant compared to wt retinas (Fig. 3B), and the percentage of cells assigned to each subcluster differed between wt and the mutants (Fig. 3C).

Cones are usually classified according to the type of opsin they express. In human previous work has described cones expressing solely S- or M-opsins, but in mouse, a high proportion of cones co-express both types of opsins (Swaroop et al., 2010). Indeed, we could classify cones by their opsin expression pattern (Supplementary Fig. 6). In the wild-type mouse retina, as much as 64% of all cones co-express both opsins, with close to 20% of cones not expressing any. A detailed analysis per mutant genotype showed notable differences, with the D27 retinas showing more cones expressing a single type of opsin in detriment of the number of cones expressing the two opsin types. Nonetheless, the most striking differences are found in the DE8 retinas, which display close to half of their cones with no opsin expression and a mere 20% of cones expressing both S- and M-opsins (Supplementary Fig. 6). In the mutant retinas, the percentage of cones expressing solely S-opsin is three- (D27) to four- (DE8) fold larger than in the wildtype, highlighting that NR2E3 is relevant for controlling the final cone fate.

Of the five cone subclusters revealed by our analysis, subclusters $cone_0$, $cone_1$ and $cone_2$ are present in both the wt and the mutant samples, although their proportion differ: subcluster $cone_0$ is more abundant in the wt, while subclusters $cone_1$ and $cone_2$ are more abundant in the mutant retinas. Subcluster $cone_3$ is exclusively detected in the mutant samples, and subcluster $cone_4$ is barely detected in the wt, indicating specific alterations in the cone differentiation pathway between the mutant and wt retinas (Fig. 3B-C). We further delved into the marker genes of each cone subcluster by analysing the most frequent GO terms relevant to photoreceptor cell and retinal function (Fig. 3D). Subcluster $cone_0$ –with a higher expression of genes necessary for cone phototransduction (*Opn1sw, Arr3, Pde6h, Gngt2*)– represents a subpopulation of fully functional and differentiated cones, while subcluster $cone_1$ represents a population of hybrid cones, with both lower expression of cone-specific and concomitant expression of rod-specific genes (*Rho, Gnat1, Cngb1, Gnb1, Rp1*) (Fig. 3E and Supplementary Fig. 7). The decrease in the number of cells in cluster $cone_0$ together with the high increase in cells from subcluster $cone_1$ in mutant retinas (Fig. 3C) suggests that hybrid photoreceptors are increased in the mutant retinas in detriment of functional cones compared to wt. This enrichment in cells of subcluster $cone_1$ may account for the higher expression of rod genes in the overall cone cell population of the *Nr2e3* mutant retinas.

Cells of subclusters $cone_2$ and $cone_3$ share the expression of a group of genes involved in retina development that are not expressed in subclusters $cone_0$ and $cone_1$, including *Kmt2a*, *Rpgrip1* and *Dmd* (Fig. 3E and Supplementary Fig. 7) (Brightman et al., 2018; Persiconi et al., 2020; Sun et al., 2022). We considered that subcluster $cone_3$ (exclusive of the mutants) is derived from subcluster $cone_2$: they both correspond to photoreceptor precursor cells (PPCs) already determined to the default cone fate (since they express high levels of S-opsin), but whose transcription signature differs due to NR2E3 misfunction and/or misexpression (Fig. 3E).

Finally, cells from subcluster $cone_4$ –mostly restricted to the mutant retinas– are likely degenerating in response to stress, as shown by apoptosis gene expression in GO term analysis (Fig. 3D) and high expression of the necrosis-associated gene *Cathepsin B* (Fig. 3E). Notably, all these stressed cones are M-cones (Fig. 3E) that show high ectopic expression of rod genes (including *Nr2e3*). These traits are also shared with the handful of $cone_4$ cells detected in the wt (Supplementary Fig. 7).

To sum up, single-cell transcriptomic analysis revealed a non-uniform cone population in wt retinas, conformed by a continuum of cells in three main stages, with a high proportion of differentiated cones (subcluster $cone_0$, average of 70% of all analysed cone cells), around 20% of hybrid cone cells (subcluster $cone_1$), and a low number of precursor cones (subcluster $cone_2$, 10%). In contrast, in the *Nr2e3*-mutant retinas the ratios appear to have shifted: the proportion of fully differentiated cones is around 20%, hybrid cones represent 40–50%, and cone cells in an early stage of differentiation (subclusters $cone_2$ and $cone_3$) account from 15% to 50% of all cones. Finally, subcluster $cone_4$ is formed by M-opsin cones expressing stress and death markers.

3.4. RNA velocity analysis unveils a population of rods in mutant retinas "transitioning" towards the cone cluster

Similarly to the cone cell population analysis, a subclustering of rod cells (Supplementary Data 3) identified eight subpopulations (Fig. 4A). Despite the significant difference in the total number of rod cells (approximately 60% fewer rods in the mutants than in the wt; Fig. 4B-C), the relative percentage of cells within each rod subcluster remains somewhat similar between all genotypes (Fig. 4C), and we could not detect genotype-specific rod subpopulations.

Highly expressed marker genes from subcluster rod_0 contain frequent GO terms associated with ribosomal and mitochondrial functions, indicative of highly metabolic populations in the retina (Supplementary Fig. 8 A) (Lidgerwood et al., 2021), which require ribosomal activities for protein synthesis and mitochondria for energy. On the other hand, marker genes from other rod subclusters contain GO terms associated with other pathways unrelated to metabolism, indicating two main populations of rods differing in their metabolic activity (Supplementary Fig. 8 A).

Rod-specific genes (*Gnat1, Rho*) were detected in all 8-rod subclusters, although this expression is decreased in subcluster rod_5 (Fig. 4D, Supplementary Fig. 8B). The misexpression of cone-specific genes (*Gnb3, Pde6h, Gnat2*) in nearly all subclusters is only detected in mutant retinas, although it is more prominent for the Δ27 samples (Supplementary Fig. 8B). In agreement with previous studies (Aísa-Marín et al., 2020a), *Nr2e3* expression was increased in the Δ27 rods and decreased in the ΔE8 rods, in which we only see expression

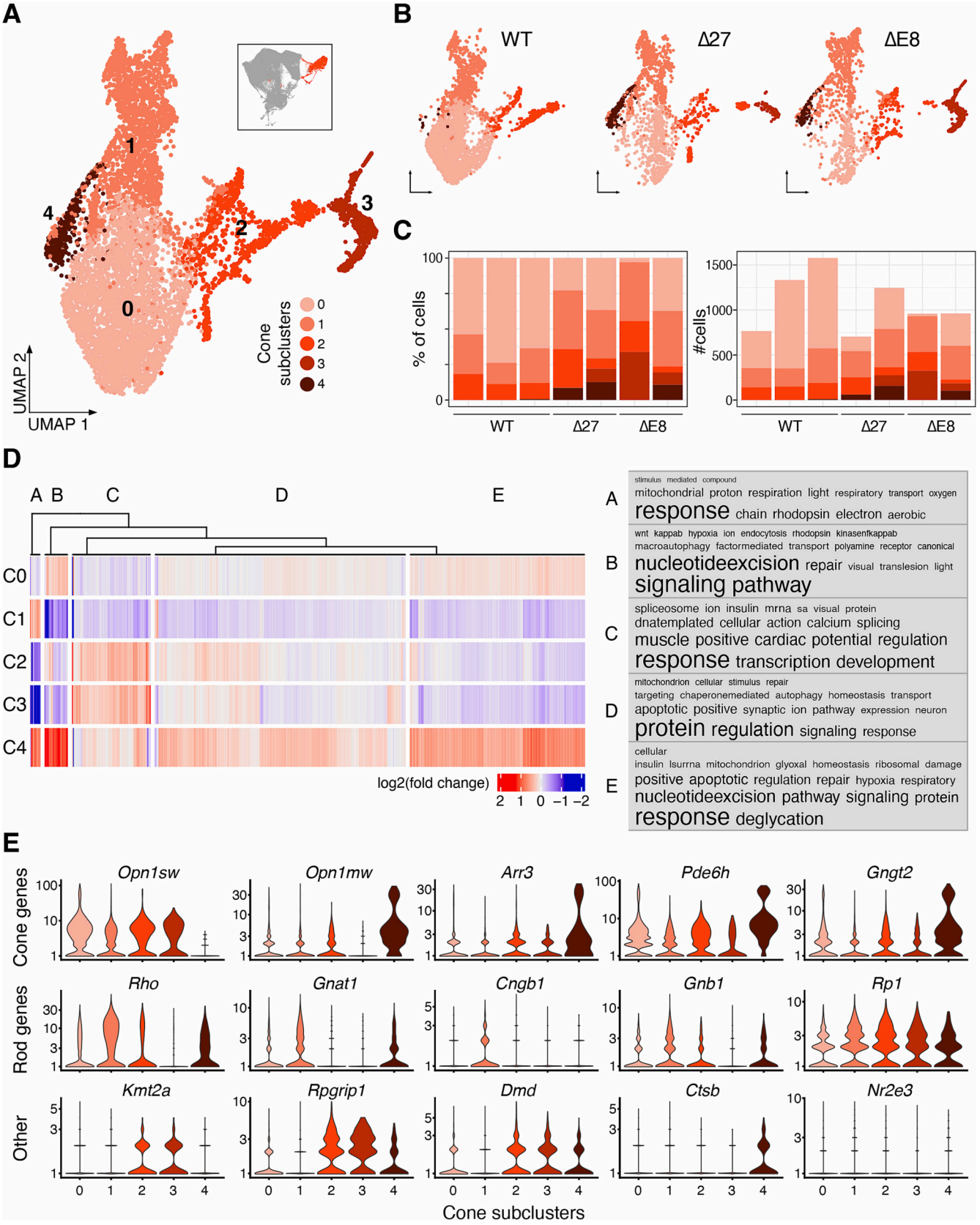

(caption on next page)

Fig. 3. Distinct subpopulations of cones are found in the Nr2e3 wildtype and mutant retinas. A. Global UMAP plot of the three genotypes identifying 5 subclusters within the cone population cluster. Each subcluster is indicated with a different shade of salmon-red. Cone cells are highlighted from the rest of the cell-types in the miniature UMAP insert (as it appears in Fig. 1B). B. Differences in the UMAP plot by genotype. Note the different burdeos-coloured subcluster at the right in the mutant retinas. C. Differences in the percentage of cells in each subcluster per individual. Subcluster $cone_0$ is more represented in the wt retina, whereas subcluster $cone_1$ is enriched in the mutants. Subclusters $cone_3$ and $cone_4$ are almost exclusive of the mutant retina samples. D. Log 2-fold change heatmap of cone subcluster marker genes sorted by k-means clustering. Frequent biological process GO terms appear in the word cloud according to their cluster. Larger font size indicates higher abundance of the GO term. E. Identification and assignment to different cone subtypes are based on the expression of specific markers. Subcluster 0 overexpress differentiated cone genes, whereas subcluster $cone_1$ overexpresses rod genes. Subclusters $cone_2$ and $cone_3$ overexpress genes related to retinal development, and subcluster $cone_4$, which correspond to M-cones in the *Nr2e3* mutants, also expresses markers associated with neuronal degeneration and cell death. (See also Supplementary Fig. 7). (For interpretation of the references to colour in this figure legend, the reader is referred to the web version of this article.)

(corresponding to the *Nr2e3* short isoform) in subcluster rod_3 (Fig. 4E). We observed an increase in S-opsin expression (*Opn1sw*) in subcluster rod_5, a cluster characterized by a lower expression of rod genes than the other rod subpopulations (Fig. 4E), which suggests that this subcluster contains hybrid rods.

Note that while scRNA-seq provides static information of cellular states at a point in time, it does not directly inform about the dynamic transcriptional processes taking part in the different cell populations. We thus used RNA velocity analysis to determine and compare the gene-splicing maturation dynamics in cell populations between the different retinas. In adult retinas, and common to all genotypes, we observe a subpopulation of S-cones transitioning towards the rod cluster (Fig. 4F arrowhead A, Supplementary Fig. 9), in agreement with the known population of rods that derive from S-cone progenitors during mouse retina development (Kim et al., 2016). Besides, the subpopulation of cones previously identified as PPCs (subclusters $cone_2$ and $cone_3$) show a strong directional flow towards the differentiated cones, confirming our previous assignment (Figs. 3, 4F arrowhead B).

Comparing the results of the RNA velocity analysis of wt and mutant retinas, we identified a population of rods in both mutants showing a strong directional flow towards the cone cluster. This trend is higher for the ΔE8 (Fig. 4F arrowhead C), indicating that this rod subpopulation could be "transitioning" towards the canonical cone pathway. Another relevant difference, particularly in the ΔE8 mutant, is the detection of strong RNA dynamic flows within each main cell type population towards the cone cluster.

3.5. Retinal remodelling processes in post-synaptic and glial cells occur in response to photoreceptor degeneration

In addition to the effect of NR2E3 misfunction in photoreceptor cell populations, we also analysed potential alterations in other main retinal cell types (Fig. 5A). The RPE cluster only presented a small number of DE genes, whereas glial, rod bipolar and the progenitor cell (RPC) clusters showed more relevant changes in gene expression in both mutants (Fig. 5B). For instance, rod bipolar cells showed underexpression of genes involved in oxidative stress and DNA repair pathways in contrast to the higher expression of this set of genes in glial cells (Fig. 5A group B). These changes are likely to be secondary to photoreceptor alteration since *Nr2e3* is not reported to be expressed in these cell types. As occurred in the rod and cone cell populations, retinal cells from the Δ27 mutant showed a higher number of DE genes compared to those of ΔE8 (Fig. 5B). For instance, Δ27 retinas show a 1.5-fold increase in the number of DE genes in the glia and rod bipolar clusters compared to ΔE8, whereas in rod bipolar cells, for some genes, the Δ27 mutants show a 15-fold increase (more than one order of magnitude) compared to ΔE8 (Fig. 5B). The high transcriptomic alteration of the Δ27-rod bipolar cells may explain the decreased functionality observed in the whole retina of Δ27 mutants, not yet detected in the young adult ΔE8 mutants even though they have similar –although less pronounced– changes in photoreceptor cells.

High overexpression of crystallin (Cry) genes was also detected in the glial cell cluster of the Δ27 compared to wt or ΔE8 retinas (Fig. 5A group A, Fig. 5C). Comprising two families, α- and βγ-crystallins are the most prevalent proteins in the lens. The expression of crystallins is susceptible to modulation in response to stress since their expression increase (Cavusoglu et al., 2003; Dufour et al., 2003; Kapphahn et al., 2003; Sakaguchi et al., 2003; Yoshimura et al., 2003) or decrease (Cottet et al., 2006) in different models of retinal stress. Although their precise function out of the lens has yet to be determined, they have been proposed as retinal stress proteins and are considered retinal remodelling markers (Andley, 2007; Templeton et al., 2013). Overexpression of *Cryaa* and *Crybb2*, belonging to the two crystallin families, was confirmed by RT-PCR (Fig. 5D-E) and Western Blot (Fig. 5F). Colocalization of CRYBB2 and the microglia cell marker IBA1 in Δ27 primary retinal cultures was also observed (Fig. 5G), supporting the hypothesis that the expression of crystallins in glial cells might reflect an induced response to retinal stress.

DE genes between mutants and wt revealed that RPCs in the mutants have lower expression of energy metabolism and mitochondrial genes associated with neuronal function, and overexpression of genes related to differentiation and developmental genes (Fig. 5A groups F and C, respectively). Additionally, Δ27 retinas frequently show processes associated with anomalous metabolism like metabolic process, glycolysis, regulation of translation and rRNA processing (Fig. 5A groups A, B and D). Overall, these results support that the alterations observed in Δ27 mutant photoreceptors also affect other retinal cell types, particularly rod bipolar and glial cells.

3.6. Some photoreceptor subpopulations in Nr2e3 mutant retinas overexpress biomarkers associated to cell damage and regulated necrosis

Apoptosis is considered the most common programmed cell pathway. Nonetheless, retinal degeneration in the Δ27 and ΔE8 mutant retinas was shown not to be caused by this cell death pathway (Aísa-Marín et al., 2020a). Notably, *Ctsb* expression is particularly upregulated in the subcluster $cone_4$, corresponding to M-cones (Fig. 3E) that also express other damage and cell death-associated genes (Fig. 3D, group E) *Cstb* encodes *Cathepsin B* (CTSB), whose overexpression has been recently associated with regulated necrosis, a form of non-apoptotic cell death in some cell types (Vanden Berghe et al., 2014; Kuang et al., 2020). To confirm the expression of CTSB in the M-cones in the mutant retinas, we performed immunohistochemistry in retinal sections (Fig. 6A). Our results confirmed that CTSB was preferentially expressed in M-cones compared to S-cones, and that CTSB expression was increased in the cone-rich invaginations characteristic of the *Nr2e3* mutant retinas (Fig. 6A).

Impaired oxidative phosphorylation (OXPHOS) is associated to mitochondrial dysfunction and may trigger necrrosis (Fatokun et al., 2014; Koo et al., 2015; Murata et al., 2019; Nagley et al., 2010). As transcriptional alteration of mitochondrial genes (including energy metabolism and mitochondrion homeostasis pathway genes) were detected in the *Nr2e3* mutant photoreceptors (Fig. 2A, Supplementary Table 2), we sought to confirm these results. The Δ27 mutant retinas showed a decrease in VDAC expression (Fig. 6C), thus suggesting mitochondrial mass reduction. Downregulation of several components of the OXPHOS chain associated with mitochondrial metabolism was also observed in the Δ27 and ΔE8 retinas (Fig. 6C-D). In summary, *Nr2e3* mutants show alterations in the protein levels of some mitochondrial biomarkers, with reduced mitochondrial mass in the Δ27

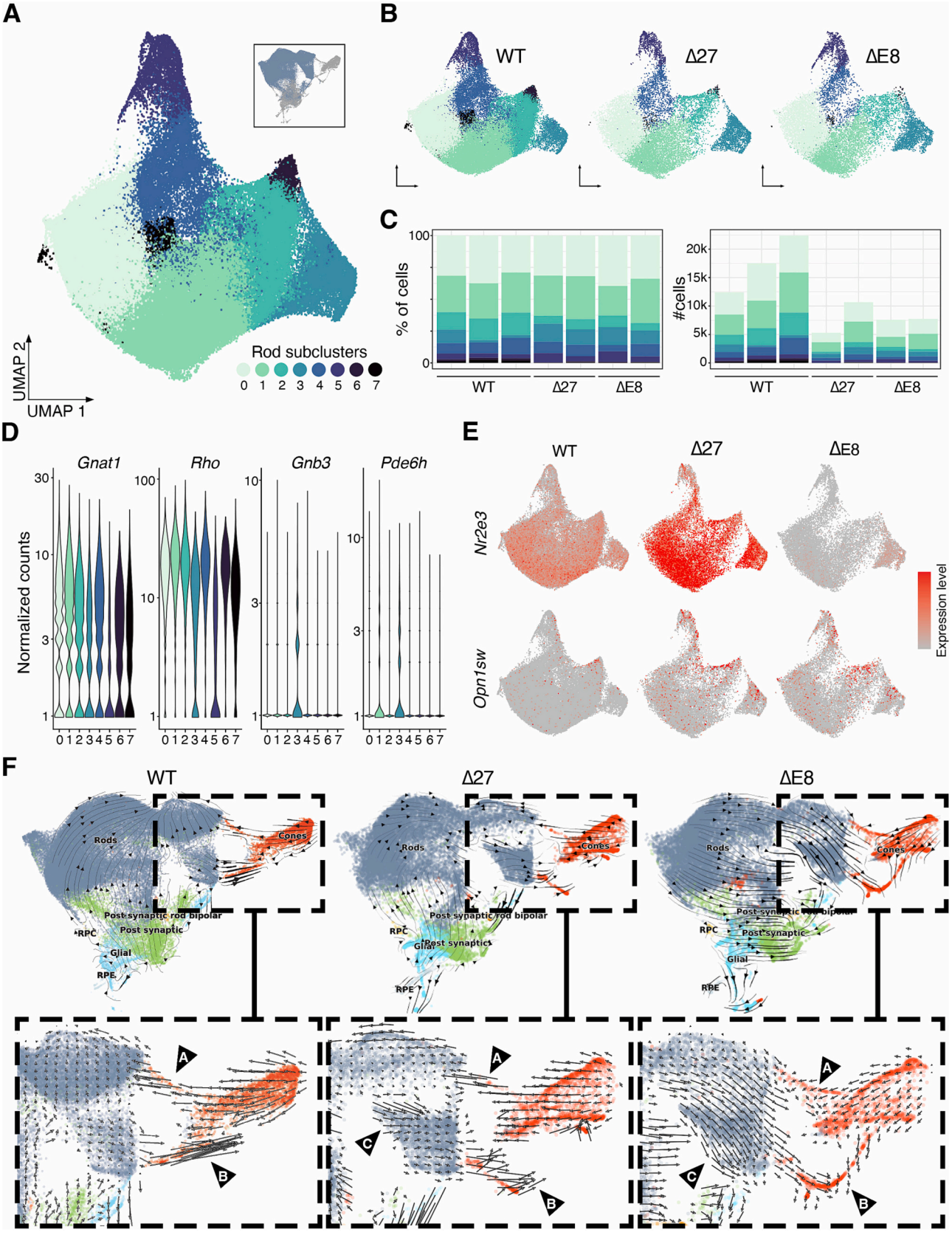

(caption on next page)

Fig. 4. RNA velocity analysis unveils a population of rods in mutant retinas "transitioning" towards the cone cluster. A. Global UMAP plot of the three genotypes identifying 8 subclusters within the rod population cluster. Each subcluster is indicated with a different shade of green-blue. Rod cells are highlighted from the rest of the cell-types in the miniature UMAP insert (as it appears in Fig. 1B). B. Differences in the UMAP plot by genotype show a decrease in the number of rods in the Δ27 and ΔE8 retinas. C. The contribution of each rod subtype (percentage) to the main rod cluster is maintained in all genotypes (left). Δ27 and ΔE8 *Nr2e3* mutant retinas show a 2-fold decrease in the number of rods compared to the wt (right). D. Expression of rod and cone genes in the rod subclusters reveals a population (subcluster rod_5) with low expression of rod genes. E. UMAP plot by genotype shows the expression of *Nr2e3* and *S-opsin* in the rod subclusters. *Nr2e3* is upregulated in the Δ27 rods and downregulated in the ΔE8 rods. Of note, in ΔE8, only the subcluster rod_3 shows the expression of the *Nr2e3* short isoform. Expression of *S-opsin* is only detected in mutant rods, mainly in subcluster rod_5. F. RNA velocity analysis of the three genotypes identifies (see inset magnification below), a subpopulation of cones showing a strong flow towards the rod cluster (A arrowheads); a subpopulation of cones –concurring with the PPCs– transitioning to fully differentiated cones in the three genotypes (B arrowheads); and a population of rods, which is differentiating towards cones, or tends to acquire cone features (arrows directed towards the cone cluster), exclusively in the mutants (C arrowheads). See also (Supplementary Figs. 8 and 9). (For interpretation of the references to colour in this figure legend, the reader is referred to the web version of this article.)

retinas and a lower number of functional mitochondrial complexes in the ΔE8 retinas, pointing to alterations in mitochondrial respiration as a plausible inducer of overexpression of cell damage and cell death-associated proteins.

We also analysed the expression of proteins associated to other specific necrotic mechanisms –such as necroptosis and parthanatos– that could be additionally involved in photoreceptor degeneration in the mutant retinas (Fig. 6D). Immunodetection of phosphorylated MLKL (ph-MLKL), involved in the necroptotic pathway) showed differences between *Nr2e3* wt and mutant retinas. In the wt retina, ph-MLKL was detected in small puncta in the cytoplasm, where it is reported to associate with endosomes and assist in endosomal transport and vesicle release (Yoon et al., 2017). In the Δ27 and ΔE8 mutant retinas, MLKL was aggregated into larger cytoplasmic clusters that accumulated at the plasma membrane (Fig. 6E), where they have been described to compromise membrane integrity and cause cell death (Samson et al., 2020). On the other hand, parthanatos is a form of programmed cell death characterized by the overactivation of PARP-1, which uses NAD+ and ATP to synthesize PAR (Fatokun et al., 2014). Therefore, PAR accumulation is commonly used to detect parthanatos. In the Δ27 mutant retinas, there was an increase in the PAR staining in the inner segment of photoreceptors, inner nuclear (INL) and ganglion cell layers (GCL) (Fig. 6E). In contrast, the ΔE8 mutant retinas showed PAR levels comparable to those of the wt in the flat (without invaginations) regions of the retina compared to an increased signal in the cone-rich invaginations.

These results are interesting but still very preliminary and require further work to dissect the potential involvement of alternative necrotic pathways in the retinal dystrophy/retinal neurodegeneration shown by our *Nr2e3* mutants.

4. Discussion

Nr2e3 mutants display the same seven major cell types identified in the wt retinas. However, both types of photoreceptors –rods and cones– show misregulation of rod and cone phototransduction genes in the Δ27 and ΔE8 mutant retinas, probably associated to the fact that they cannot produce the functional long isoform of *Nr2e3*, which includes the domains involved in the dimerization and transcription repression activity. Therefore, the NR2E3 role as a repressor of cone-specific genes is most probably impaired, and as a result, cone genes are overexpressed in both rod and cone photoreceptor populations. Rod genes are also overexpressed in the rod and cone clusters since the NR2E3 protein expressed in the mutants still retains the transactivating activity. The upregulation of rod genes is more notable in the Δ27 mutant, in accordance with the high overexpression of *Nr2e3* in the Δ27 compared to the ΔE8 mutant, more akin to a knockdown *Nr2e3* model. Misregulation of phototransduction genes generates hybrid photoreceptors, in which both rod- and cone-specific genes are expressed in the same cell type. These results are in agreement to the hybrid photoreceptor cells expressing both rod and cone genes reported in the *rd7* mouse (Corbo and Cepko, 2005), and the reports on cone/rod intermediate populations –termed *cods*– in retinal organoids from a *NRL*-null patient showing an ESCS phenotype (Kallman et al., 2020).

Although NRL is the main transcription factor for rod differentiation, NR2E3 is required to secure and maintain rod photoreceptor commitment and homeostasis. Therefore, a substantial decrease in the number of rods is detected in the *Nr2e3* mutant compared to the wt retina. Several reasons can explain this decrease in the rod number: (i) a global reduction in the number of rods generated during the development (at the expense of an increased number of cones), (ii) the misfunction and subsequent degeneration of the existent rods, or (iii) a combination of both.

During mammalian retina development, photoreceptor precursors (PPCs) follow a default pathway to differentiate into S-cones unless other regulatory signals determine them towards the rod or M-cone identity (Swaroop et al., 2010). In addition to rods originating from rod precursors, some mature rods derive from a pool of PPCs initially expressing S-opsin, which redirect their fate towards the rod pathway, demonstrating the plasticity of initial S-cone photoreceptors (Kim et al., 2016) (graphic model in Fig. 7A). Some authors hypothesize that the increase in the number of S-cones observed in the *Nr2e3* mouse mutants comes from the fraction of rods derived from the default S-cones that fail to differentiate into mature rods due to lack of functional NR2E3 (Coppieters et al., 2007; Xie et al., 2019). Other authors instead hypothesize that the increase in the number of S-cones –as that observed in the Δ27 and ΔE8 mutants (3 to 4 fold higher in the mutants if considering the cones expressing solely S-opsin)– may arise from photoreceptors committed to the rod pathway that transition towards cone fate instead of arising from the particular population of rods derived from PPCs expressing S-opsin. The RNA velocity analysis in our retina samples detects a strong flow from the S-cone population to the rod cluster in both the wt and the mutants, consistent with the subpopulation of default S-cones differentiating into rods. Nonetheless, we also observe a transition flow from the rod population towards the cone cluster (graphic model in Fig. 7A). Therefore, our data supports both pathways, as shown in the comprehensive model of the effect of *Nr2e3* mutations (Fig. 7B).

One of the main conclusions from our single-cell retinal analysis is that cones and rods are not homogeneous populations of photoreceptor cells but instead present a continuum of differential phenotypes. The use of marker genes allowed the identification of these different subpopulations within the largely heterogeneous rod and cone clusters. Other authors had already identified rod subpopulations that differ in their direct synaptic contacts (Tsukamoto et al., 2001). Our data further dissects the large rod population by identifying a subpopulation of rods characterized by high metabolic requirements, as indicated by increased expression of ribosomal and mitochondrial genes. The presence of distinct rod subpopulations might result from specific adaptations to different requirements.

Interestingly, although the number of rods is significantly decreased in the mutants, the number of subclusters is similar between the three genotypes, and only the percentage of cells in each subcluster varies. These results suggest that mutations in *Nr2e3* cause a shift of cells among rod subpopulations, rather than adding or subtracting specific subpopulations. The similar number of subclusters can be explained if: (i) all

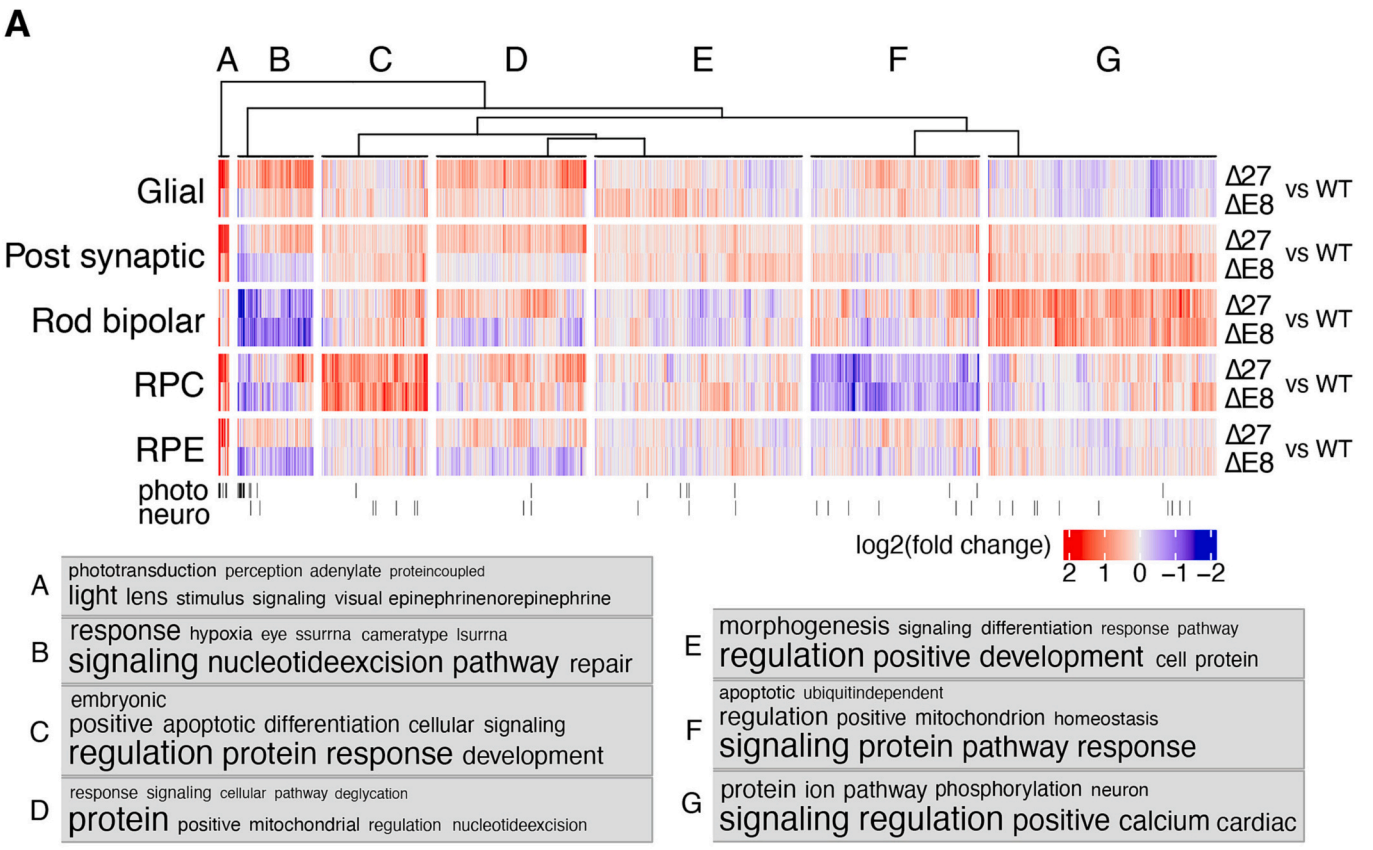

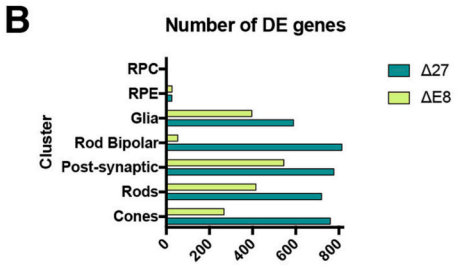

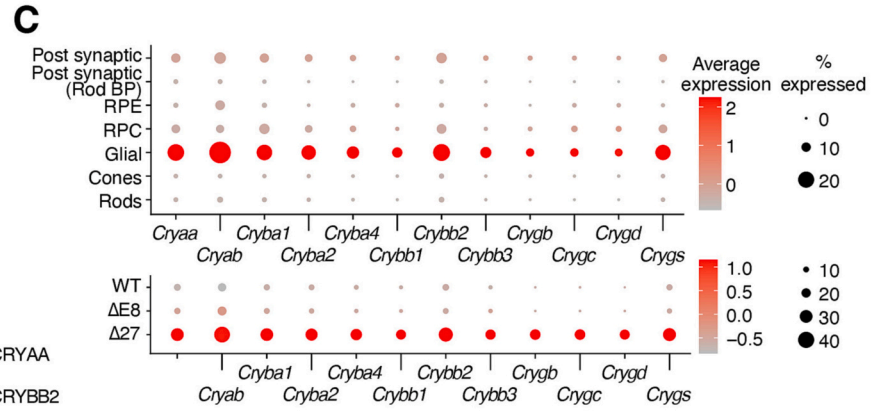

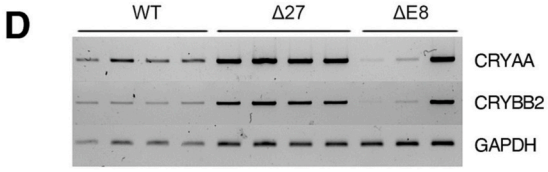

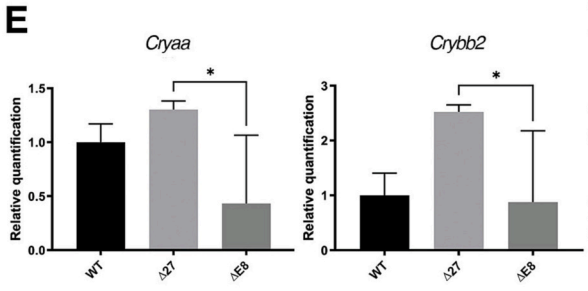

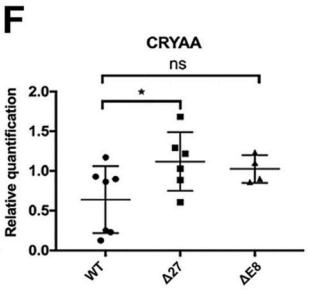

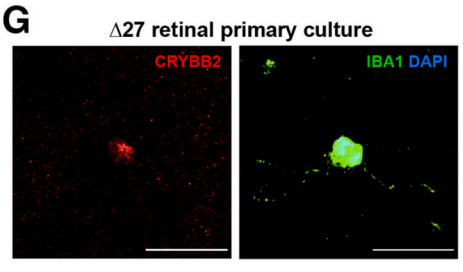

(caption on next page)

Fig. 5. Altered gene expression in *Nr2e3* mutant photoreceptors impact in other neuronal layers and indicate extensive retinal remodelling processes affecting glial, bipolar and progenitor cells. A. Log 2-fold change heatmap of DE genes in different retinal cell types in Δ27 and ΔE8 mutants vs wt retinas sorted by k-means clustering. Frequent biological process GO terms appear in the cloud according to their presence in each cluster. Larger font size indicates higher abundance of the GO term. Photo and Neuro indicate specific photoreceptor and neuronal genes, respectively. B. Number of DE genes in the mutant vs wt retinas in the seven main cell type clusters. Note that the number of DE genes is higher in the Δ27 retinas compared to the ΔE8 retinas. C. Dot plot showing average and percentage expression of several genes of the crystallin (cry) family in the seven main cell type clusters (upper panel). The expression of Cry genes, indicative of retinal stress, is increased in the glial cell cluster in the Δ27 mutants (bottom panel). D, E. *Cryaa* and *Crybb2* overexpression were validated by RT-PCR of retinal lysates. Samples correspond to independent biological replicates from the three genotypes (Lanes 1–4 wt, 5–8 Δ27, 9–11 ΔE8). (statistical significance, $*p < 0.05$, Kruskal-Wallis test). F. CRYAA overexpression was also quantified by Western Blot of retinal lysates ($n = 4$–7) (statistical significance, $*p < 0.05$, one-way ANOVA test). In (E, F) data are presented as mean and SD. (See details of age and sex for (D—F) in Material and Methods). G. Immunocytochemistry of Δ27 primary retinal cell cultures (P0–1) show co-expression of CRYBB2 (red) and IBA1 (staining microglia, green) in the same cell, confirming the expression of cry genes, indicative of stress-associated remodelling in the glia. (For interpretation of the references to colour in this figure legend, the reader is referred to the web version of this article.)

subtypes of rods degenerate uniformly, or (ii) rod population may be dynamic, with a flexible modulation between the distinct types of rods. Thus, the rod differentiation pathway is not directly affected by mutations in *Nr2e3*, which reinforces the role of NR2E3 in both maintaining –but not directly promoting– the differentiated rod fate and favouring rod survival.

In contrast, *Nr2e3* mutations –at least in young adult retinas– have a larger and more relevant impact on the composition and identity of cone subclusters since the proportions between the different cone subpopulations are inverted, and new subclusters appear as exclusive or nearly exclusive of mutant retinas. Indeed, the percentage of cones expressing either S- or M-opsins, or co-expressing both differs between wild-type and the *Nr2e3* mutants, probably due to defects in the cone differentiation pathway. For instance, in the ΔE8 mutant, half of the population of cones does not express neither S-nor M-opsin. The number of fully differentiated cones diminishes whereas subpopulations of hybrid cones or precursor cone cells are much enriched in the mutant retinas, accounting for up to 70% of all cone cells.

Of note, our results indicate that *Nr2e3* mutations cause selective M-cone expression of proteins associated to regulated necrosis, a common form of non-apoptotic cell death. In fact, there is increasing evidence that alternative cell death mechanisms different from apoptosis play a major role in retinal neurodegeneration (Arango-Gonzalez et al., 2014; Yan et al., 2021). Prior studies detected non-apoptotic cell death markers in the *rd7* mouse model (Venturini et al., 2021). We here specifically identified expression of markers associated to alternative necrotic pathways, unreported in the *Nr2e3* mutant retinas up to now. Together, these results indicate that several non-apoptotic cell death pathways might be activated as a consequence of the loss of function of NR2E3. However, the specific mechanisms by which degeneration might occur and why it seem to affect M- versus S-cones remains unknown and deserve further work. ESCS patients show increased S-cone and decreased M- and L-cone sensitivities, although this varies among individuals (Ripamonti et al., 2014). Together with data obtained in zebrafish (Xie et al., 2019), our results suggest that the decreased M- and L-cone sensitivities in ESCS patients might be due to a combination of both, the increased number of S-cones and the selective loss of M- and L-cones, as a consequence of *NR2E3* mutations.

In response to photoreceptor deterioration, the retina suffers a process of negative plasticity called retinal remodelling, which comprises multiple mechanisms like alterations in retinal metabolism and neuronal network topologies (Jones and Marc, 2005; Jones et al., 2016; Pfeiffer et al., 2020). We hypothesize that retinal remodelling occurs in the *Nr2e3* mutants, as suggested by the frequent GO terms in specific pathways in the rod bipolar and glial cells, particularly in the Δ27 retinas, which also show overexpression of the *cry* family of genes triggered in response to stress. In fact, all the observed expression alterations are more pronounced in the Δ27 than in the ΔE8 mutants, not only by the increased gene misexpression in rods and cones but also by the higher number of DE genes in all cell types, particularly bipolar cells, highly indicative of extensive retinal remodelling in the Δ27 retinas.

Concerning human disease, the Δ27 is a model of the ESCS whereas the ΔE8 retina shows a late-onset RP phenotype (Aísa-Marín et al., 2020a). Our data suggest that the ECSC-like retinal dystrophy detected in the Δ27 retinas at early stages is mostly due to this early-onset retinal remodelling rather than to rod/cone gene misexpression, as young ΔE8 retinas, which also show gene misexpression, only display slightly reduced responses in rod cells (Aísa-Marín et al., 2020a). Therefore, and according to our proposed model (Fig. 7), mutations that allow NR2E3 to still retain some function (as might happen in the Δ27 model) might exert a dominan-negatve effect causing an early-onset but stable retinal remodelling, whereas loss of function/knockdown mutations (as in ΔE8) would instead mainly affect photoreceptor homeostasis and survival, causing progressive photoreceptor attrition and leading to a more severe RP-like phenotype at later stages.

Overall, our results support that *Nr2e3* misfunction: a) causes transcriptional misregulation of cone and rod marker genes, and changes photoreceptor fate, with an enrichment in hybrid cones; b) demonstrates that cone and rod populations are not homogeneous but composed of different subpopulations with specific requirements and transcriptional signatures; c) indicates that photoreceptor differentiation is not a strict and mutually exclusive process that generates either rods or cones –even in the wt retinas–, but there is instead a hybrid photoreceptor subpopulation that can be directed towards either fate; and d) demonstrates that high overexpression of rod and cone genes in the same cell compromises photoreceptor identity, leading to degeneration, probably through necrotic pathways.

Our work, performed in mouse retinas, should be further replicated and confirmed in human-derived models (e.g. retinal organoids). Nonetheless, considering our results, we propose that photoreceptor fate commitment and/or photoreceptor homeostasis might be differentially affected depending on the *NR2E3* mutation, thus leading to either the ECSC or the RP phenotype.

Funding

I.A.-M. is recipient of the APIF grant (Universitat de Barcelona), and the Company of Biologists grant for short term mobility. This research was supported by grants PID2019-108578RB-I00 and PID2022-140957OB-I00 (MCIN/AEI/10.13039/501100011033/FEDER), 2021 SGR738 (Generalitat de Catalunya) to G.M. Work in the Vaquerizas laboratory is supported by the Medical Research Council, UK (award reference MC_UP_1605/10 to J.M.V.), the Academy of Medical Sciences and the Department of Business, Energy and Industrial Strategy (award reference APR3\1017 to J.M.V.).

Authorcontributions

I.A.-M. and Q.R. have performed the experiments, analysed the data; designed figures and written the draft manuscript; N.D. and L.C. have contributed to some figures; J.M.V. and G.M. provided the initial concept and funding, have supervised the work and analysed the data. All authors have revised the manuscript.

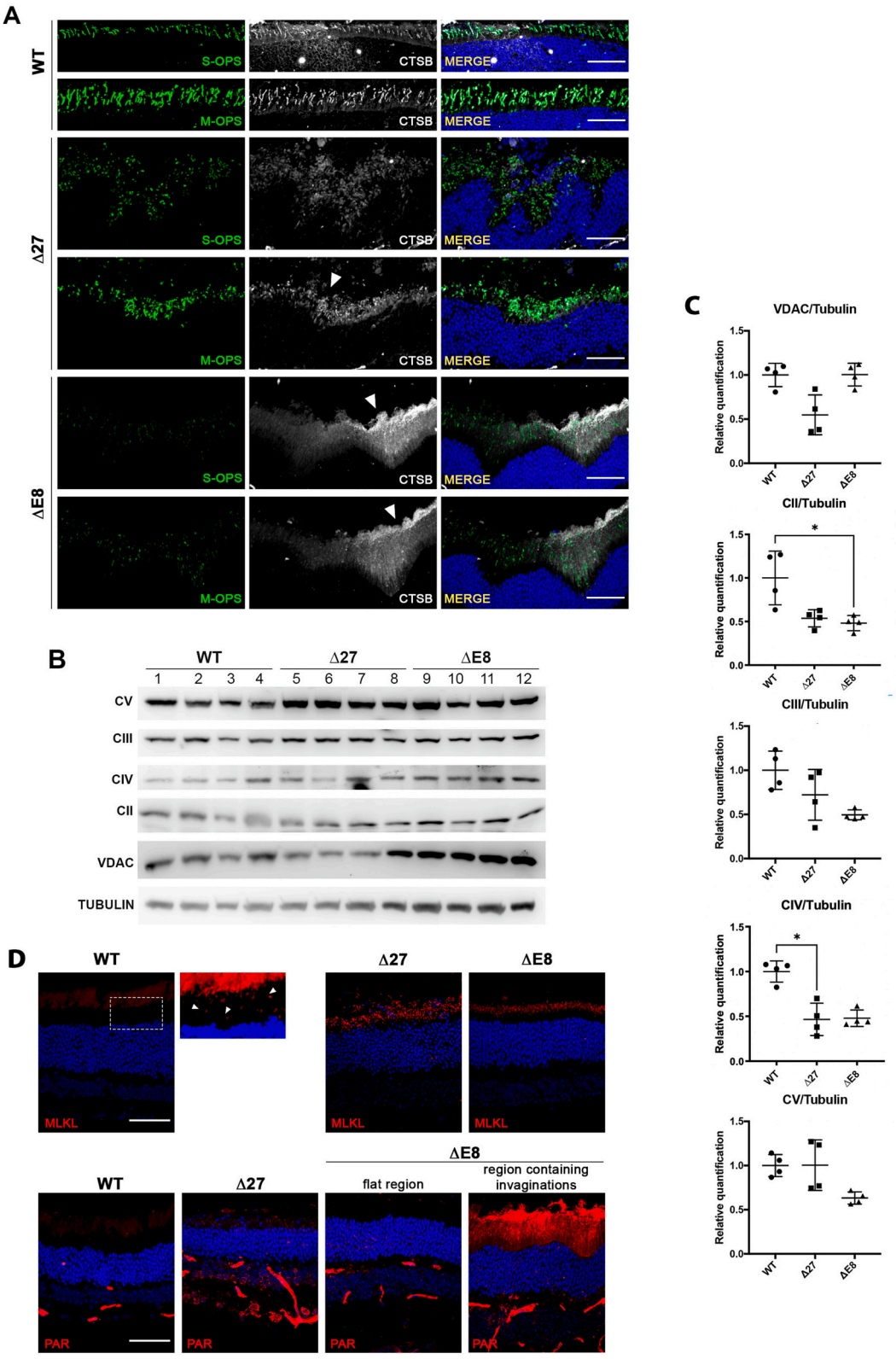

Fig. 6. Higher expression of Cathepsin B, phosphorylated MLKL and PAR as well as mitochondrial alterations are detected in the *Nr2e3* mutant retinas. A. Immunostaining of Cathepsin B (CSTB) and (B) colocalization with M- and S-opsins (in green) reveals increased CTSB expression in the M-cones compared to S-cones in all genotypes. Note the CSTB expression in the cone-rich invaginations in the mutant retinas (white arrowheads). B. Immunodetection and (C) quantification of VDAC and mitochondrial OXPHOS complex proteins reveals reduced mitochondrial mass (VDAC/tubulin) in the Δ27 retinas, and lower protein levels of some OXPHOS complexes, indicating mitochondrial alterations in the mutant retinas. Data are represented as mean and SD. (statistical significance, $*p < 0.05$, Kruskal-Wallis test). D. ph-MLKL and PAR immunostaining (considered as biomarkers of necroptosis and parthanatos) reveal an increased signal in the Δ27 and ΔE8 mutant retinas compared to wt. Note that staining of PAR antibody in the INL, IPL, and GL of the retina corresponds to background unspecific staining due to binding of the secondary anti-mouse antibody to the endogenous IgG antibodies circulating in the blood vessels. (For interpretation of the references to colour in this figure legend, the reader is referred to the web version of this article.)

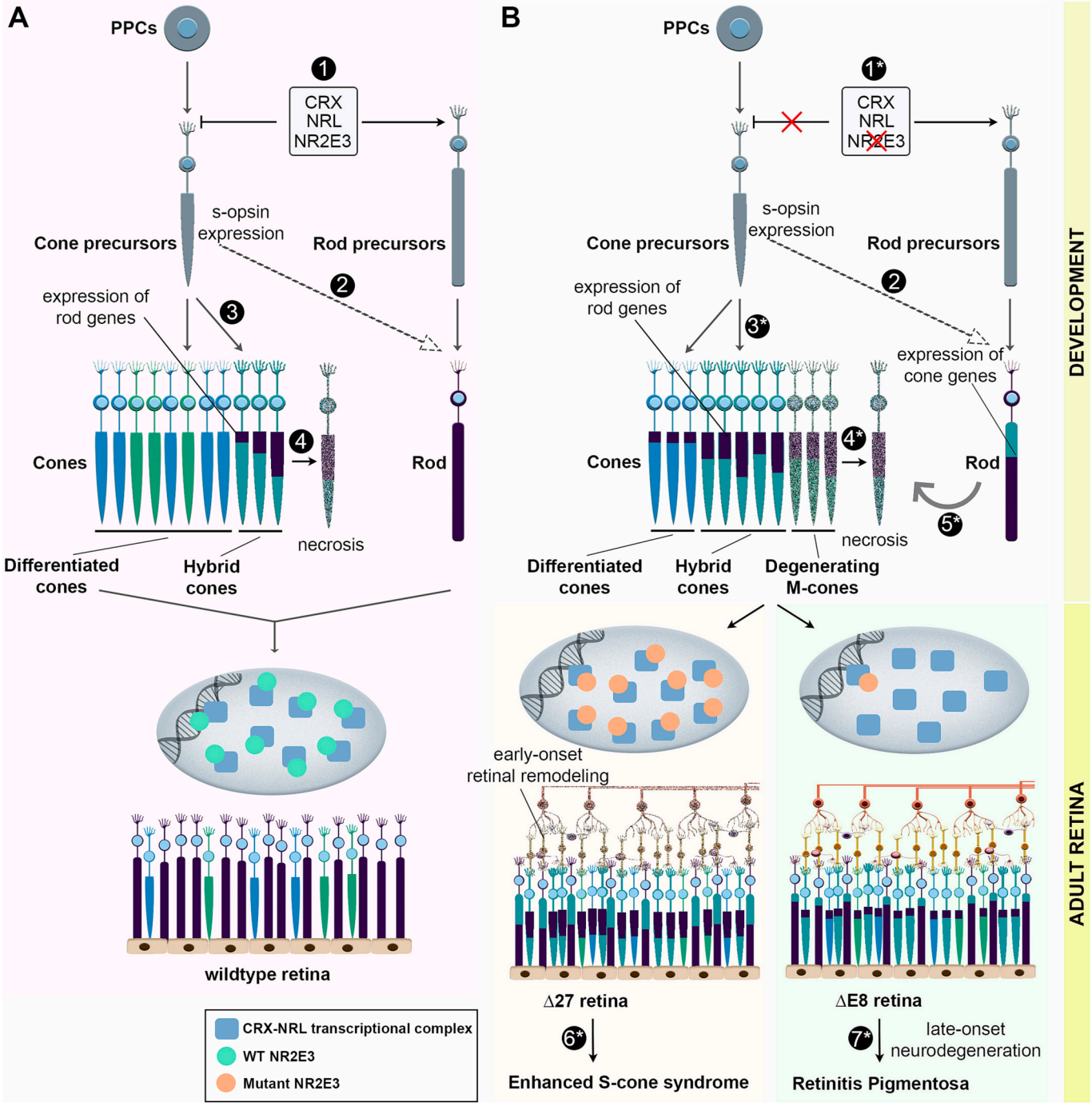

Fig. 7. Proposed model for NR2E3-associated disease mechanisms. A. During the development of the wt retina, NR2E3 contributes –together with CRX and NRL– to both repression of the cone default pathway and activation of rod genes, thus committing photoreceptors towards the rod fate (1). A fraction of cone precursors expressing S-opsin also contribute to the rod population (2), while most cone precursors differentiate into S- or M-cones. The commitment to rod or cone fate is not fully mutually exclusive, and a small number of cones highly express both cone and rod genes (3). These intermediate cones degenerate via regulated necrosis (4). B. Loss or misfunction of NR2E3 due to mutations impairs securing the commitment to the rod fate; repression of cone genes partially fails while rod genes are activated, thus resulting in a population of hybrid rods (1*). The fraction of cone precursors that contribute to the rod population is maintained (2). However, the largest pool of the cone population fails to fully differentiate and become intermediate cones displaying high expression of both cone and rod genes (3*). Mutant intermediate M-cones that highly express rod genes degenerate may die via regulated necrosis (4*). Besides, in the mutant retinas, a fraction of hybrid rods transition backwards to a more cone-like state (5*). In the Δ27 retinas, with a similar phenotype to human ECSC, overexpression of the mutant NR2E3 may cause a dominant transcription factor negative effect that results in higher misexpression of rod and cone genes, which leads to retina remodelling. Some residual NR2E3 function remains and retinal degeneration proceeds more slowly (6*). In contrast, in the ΔE8 retinas, the expression of mutant NR2E3 is very low and the effect on misexpression of rod and cone genes is not as pronounced. However, the lack of NR2E3 affects photoreceptor homeostasis and results in the progressive neurodegenerative phenotype characteristic of RP (7*).

CRediT authorship contribution statement

Izarbe Aísa-Marín: Writing – original draft, Methodology, Investigation, Formal analysis. **Quirze Rovira:** Writing – original draft, Validation, Methodology, Formal analysis, Data curation. **Noelia Díaz:** Writing – original draft, Validation, Methodology, Formal analysis. **Laura Calvo-López:** Methodology, Investigation. **Juan M. Vaquerizas:** Writing – original draft, Validation, Supervision, Software, Resources, Funding acquisition, Conceptualization. **Gemma Marfany:** Writing – review & editing, Writing – original draft, Validation, Supervision, Resources, Funding acquisition, Conceptualization.

Declarationof competing interest

The authors declare no conflict of interest.

Data availability

Raw scRNAseq data is at ArrayExpress (E-MTAB-12183) and is publicly available from the date of publication. Further information for scRNASeq data to Juanma Vaquerizas (j.vaquerizas@lms.mrc.ac.uk)

Acknowledgments

We are grateful to the associations of patients affected by retinal dystrophies for their constant support, particularly Retina Asturias, and Asociación “Muévete por los que no pueden”. We also acknowledge past and present members of our research group for helpful discussions.

Appendix A. Supplementary data

Supplementary data to this article can be found online at https://doi.org/10.1016/j.nbd.2024.106463.

References

Aísa-Marín, I., López-Iniesta, M.J., Milla, S., Lillo, J., Navarro, G., de la Villa, P., Marfany, G., 2020a. Nr2e3 functional domain ablation by CRISPR-Cas9D10Aidentifies a new isoform and generates retinitis pigmentosa and enhanced S-cone syndrome models. Neurobiol. Dis. 146.
Aísa-Marín, I., López-Iniesta, M.J., Marfany, G., 2020b. Data on the generation of two Nr2e3 mouse models by CRISPR / Cas9D10A nickase. Data Br. 33, 106447.
Akhmedov, N.B., Piriev, N.I., Chang, B., Rapoport, A.L., Hawes, N.L., Nishina, P.M., Nusinowitz, S., Heckenlively, J.R., Roderick, T.H., Kozak, C.A., et al., 2000. A deletion in a photoreceptor-specific nuclear receptor mRNA causes retinal degeneration in the rd7 mouse. Proc. Natl. Acad. Sci. USA 97, 5551–5556.
Andley, U.P., 2007. Crystallins in the eye: function and pathology. Prog. Retin. Eye Res. 26, 78–98.
Arango-Gonzalez, B., Trifunović, D., Sahaboglu, A., Kranz, K., Michalakis, S., Farinelli, P., Koch, S., Koch, F., Cottet, S., Janssen-Bienhold, U., et al., 2014. Identification of a common non-apoptotic cell death mechanism in hereditary retinal degeneration. PLoS One 9, e112142.
Bales, K.L., Ianov, L., Kennedy, A.J., Sweatt, J.D., Gross, A.K., 2018. Autosomal dominant retinitis pigmentosa rhodopsin mutant Q344X drives specific alterations in chromatin complex gene transcription. Mol. Vis. 24, 153–164.
Bergen, V., Lange, M., Peidli, S., Wolf, F.A., Theis, F.J., 2020. Generalizing RNA velocity to transient cell states through dynamical modeling. Nat. Biotechnol. 38, 1408–1414.
Bernal, S., Solans, T., Gamundi, M.J., Hernan, I., De Jorge, L., Carballo, M., Navarro, R., Tizzano, E., Ayuso, C., Baiget, M., 2008. Analysis of the involvement of the NR2E3 gene in autosomal recessive retinal dystrophies. Clin. Genet. 73, 360–366.
Bocquet, B., Marzouka, N.A.D., Hebrard, M., Manes, G., Sénéchal, A., Meunier, I., Hamel, C.P., 2013. Homozygosity mapping in autosomal recessive retinitis pigmentosa families detects novel mutations. Mol. Vis. 19, 2487–2500.
Brightman, D.S., Grant, R.L., Ruzycki, P.A., Suzuki, R., Hennig, A.K., Chen, S., 2018. MLL1 is essential for retinal neurogenesis and horizontal inner neuron integrity. Sci. Rep. 8.
Butler, A., Hoffman, P., Smibert, P., Papalexi, E., Satija, R., 2018. Integrating single-cell transcriptomic data across different conditions, technologies, and species. Nat. Biotechnol. 36, 411–420.
Cavusoglu, N., Thierse, D., Mohand-Saïd, S., Chalmel, F., Poch, O., Van-Dorsselaer, A., Sahel, J.A., Léveillard, T., 2003. Differential proteomic analysis of the mouse retina: the induction of crystallin proteins by retinal degeneration in the rd1 mouse. Mol. Cell. Proteomics 2, 494–505.
Chen, J., Rattner, A., Nathans, J., 2005. The rod photoreceptor-specific nuclear receptor Nr2e3 represses transcription of multiple cone-specific genes. J. Neurosci. 25, 118–129.
Chen, J., Rattner, A., Nathans, J., 2006. Effects of L1 retrotransposon insertion on transcript processing, localization and accumulation: lessons from the retinal degeneration 7 mouse and implications for the genomic ecology of L1 elements. Hum. Mol. Genet. 15, 2146–2156.
Chen, S., Zhou, Y., Chen, Y., Gu, J., 2018. Fastp: an ultra-fast all-in-one FASTQ preprocessor. Bioinformatics 34, i884–i890.
Cheng, H., Khanna, H., Oh, E.C.T., Hicks, D., Mitton, K.P., Swaroop, A., 2004. Photoreceptor-specific nuclear receptor NR2E3 functions as a transcriptional activator in rod photoreceptors. Hum. Mol. Genet. 13, 1563–1575.
Cheng, H., Aleman, T.S., Cideciyan, A.V., Khanna, R., Jacobson, S.G., Swaroop, A., 2006. In vivo function of the orphan nuclear receptor NR2E3 in establishing photoreceptor identity during mammalian retinal development. Hum. Mol. Genet. 15, 2588–2602.
Coppieters, F., Leroy, B.P., Beysen, D., Hellemans, J., De Bosscher, K., Haegeman, G., Robberecht, K., Wuyts, W., Coucke, P.J., De Baere, E., 2007. Recurrent mutation in the first zinc finger of the orphan nuclear receptor NR2E3 causes autosomal dominant retinitis pigmentosa. Am. J. Hum. Genet. 81, 147–157.
Corbo, J.C., Cepko, C.L., 2005. A hybrid photoreceptor expressing both rod and cone genes in a mouse model of enhanced S-cone syndrome. PLoS Genet. 1 (2), e11.
Cottet, S., Michaut, L., Boisset, G., Schlecht, U., Gehring, W., Schorderet, D.F., 2006. Biological characterization of gene response in Rpe65−/− mouse model of Leber's congenital amaurosis during progression of the disease. FASEB J. 20, 2036–2049.
De Sevilla, Pérez, Müller, L., Azar, S.S., de los Santos, J., Brecha, N.C., 2017. Prox1 Is a marker for AII Amacrine cells in the Mouse Retina. Front. Neuroanat. 11.
Dufour, E.M., Nandrot, E., Marchant, D., Van Den Berghe, L., Gadin, S., Issilame, M., Dufier, J.L., Marsac, C., Carper, D., Menasche, M., et al., 2003. Identification of novel genes and altered signaling pathways in the retinal pigment epithelium during the Royal College of surgeons rat retinal degeneration. Neurobiol. Dis. 14, 166–180.
Dyer, M.A., Livesey, F.J., Cepko, C.L., Oliver, G., 2003. Prox1 function controls progenitor cell proliferation and horizontal cell genesis in the mammalian retina. Nat. Genet. 341 (34), 53–58.
Fatokun, A.A., Dawson, V.L., Dawson, T.M., 2014. Parthanatos: mitochondrial-linked mechanisms and therapeutic opportunities. Br. J. Pharmacol. 171, 2000–2016.
Gerber, S., Rozet, J.M., Takezawa, S.I., dos Santos, L.C., Lopes, L., Gribouval, O., Penet, C., Perrault, I., Ducroc, D., Souied, E., et al., 2000. The photoreceptor cell-specific nuclear receptor gene (PNR) accounts for retinitis pigmentosa in the Crypto-Jews from Portugal (Marranos),s urvivors froom the Spanish Inquisition. Hum. Genet. 107, 276–284.
Gire, A.I., Sullivan, L.S., Bowne, S.J., Birch, D.G., Hughbanks-wheaton, D., John, R., Daiger, S.P., 2007. The Gly56Arg mutation in NR2E3 accounts for 1-2% of autosomal dominant retinitis pigmentosa. Mol. Vis. 13, 1970–1975.
Haider, N.B., 2001. Excess cone cell proliferation due to lack of a functional NR2E3 causes retinal dysplasia and degeneration in rd7/rd7 mice. Hum. Mol. Genet. 10, 1619–1626.
Haider, N.B., Jacobson, S.G., Cideciyan, A.V., Swiderski, R., Streb, L.M., Searby, C., Beck, G., Hockey, R., Hanna, D.B., Gorman, S., et al., 2000. Mutation of a nuclear receptor gene, NR2E3, causes enhanced S cone syndrome, a disorder of retinal cell fate. Nat. Genet. 24, 127–131.
Hoang, T., Wang, J., Boyd, P., Wang, F., Santiago, C., Jiang, L., Yoo, S., Lahne, M., Todd, L.J., Jia, M., et al., 2020. Gene regulatory networks controlling vertebrate retinal regeneration. Science 370.
Jeon, C., Strettoi, E., Masland, R.H., 1998. The major cell populations of the mouse retina. J. Neurosci. 18, 8936–8946.
Jin, K., Jiang, H., Xiao, D., Zou, M., Zhu, J., Xiang, M., 2015. Tfap2a and 2b act downstream of Ptf1a to promote amacrine cell differentiation during retinogenesis. Mol. Brain 8.
Jones, B.W., Marc, R.E., 2005. Retinal remodeling during retinal degeneration. Exp. Eye Res. 81, 123–137.
Jones, B.W., Pfeiffer, R.L., Ferrell, W.D., Watt, C.B., Marmor, M., Marc, R.E., 2016. Retinal remodeling in human retinitis pigmentosa. Exp. Eye Res. 150, 149–165.
Kallman, A., Capowski, E.E., Wang, J., Kaushik, A.M., Jansen, A.D., Edwards, K.L., Chen, L., Berlinicke, C.A., Joseph Phillips, M., Pierce, E.A., et al., 2020. Investigating cone photoreceptor development using patient-derived NRL null retinal organoids. Commun. Biol. 3, 82.
Kanda, A., Swaroop, A., 2009. A comprehensive analysis of sequence variants and putative disease-causing mutations in photoreceptor-specific nuclear receptor NR2E3. Mol. Vis. 15, 2174–2184.
Kannabiran, C., Singh, H., Sahini, N., Jalali, S., Mohan, G., 2012. Mutations in TULP1, NR2E3 and MFRP in indian families with autosomal recessive retinitis pigmentosa. Mol. Vis. 18, 1165–1174.
Kapphahn, R.J., Ethen, C.M., Peters, E.A., Higgins, L.A., Ferrington, D.A., 2003. Modified alpha A crystallin in the retina: altered expression and truncation with aging. Biochemistry 42, 15310–15325.
Kim, J.W., Yang, H.J., Oel, A.P., Brooks, M.J., Jia, L., Plachetzki, D.C., Li, W., Allison, W. T., Swaroop, A., 2016. Recruitment of rod photoreceptors from short-wavelength-sensitive cones during the evolution of nocturnal vision in mammals. Dev. Cell 37, 520–532.
Koo, M.J., Rooney, K.T., Choi, M.E., Ryter, S.W., Choi, A.M.K., Moon, J.S., 2015. Impaired oxidative phosphorylation regulates necroptosis in human lung epithelial cells. Biochem. Biophys. Res. Commun. 464, 875–880.
Kuang, F., Liu, J., Li, C., Kang, R., Tang, D., 2020. Cathepsin B is a mediator of organelle-specific initiation of ferroptosis. Biochem. Biophys. Res. Commun. 533, 1464–1469.

La Manno, G., Soldatov, R., Zeisel, A., Braun, E., Hochgerner, H., Petukhov, V., Lidschreiber, K., Kastriti, M.E., Lönnerberg, P., Furlan, A., et al., 2018. RNA velocity of single cells. Nature 560, 494–498.
Laboissonniere, L.A., Goetz, J.J., Martin, G.M., Bi, R., Lund, T.J.S., Ellson, L., Lynch, M. R., Mooney, B., Wickham, H., Liu, P., et al., 2019. Molecular signatures of retinal ganglion cells revealed through single cell profiling. Sci. Report. 91 (9), 1–15.
Lidgerwood, G.E., Senabouth, A., Smith-Anttila, C.J.A., Gnanasambandapillai, V., Kaczorowski, D.C., Amann-Zalcenstein, D., Fletcher, E.L., Naik, S.H., Hewitt, A.W., Powell, J.E., et al., 2021. Transcriptomic profiling of human pluripotent stem cell-derived retinal pigment epithelium over time. Genomics Proteomics Bioinform. 19, 223–242.
Liu, Y.S., Pan, J.Q., Wan, J.F., Ren, C.Y., Xu, Z.H., Pan, X. Bin, Gao, R.N., Liu, S.Q., Zhang, J.L., Yao, Q.H., et al., 2020. A novel missense mutation of RPGR identified from retinitis pigmentosa affects splicing of the ORF15 region and causes loss of transcript heterogeneity. Biochem. Biophys. Res. Commun. 531, 172–179.
Luecken, M.D., Theis, F.J., 2019. Current best practices in single-cell RNA-seq analysis: a tutorial. Mol. Syst. Biol. 15.
McGinnis, C.S., Murrow, L.M., Gartner, Z.J., 2019. DoubletFinder: doublet detection in single-cell RNA sequencing data using artificial nearest neighbors. Cell Syst. 8, 329–337.e4.
Mirra, S., García-Arroyo, R., Domènech, B., Gavaldà-Navarro, A., Herrera-Úbeda, C., Oliva, C., Garcia-Fernàndez, J., Artuch, R., Villarroya, F., Marfany, G., 2021. CERKL, a retinal dystrophy gene, regulates mitochondrial function and dynamics in the mammalian retina. Neurobiol. Dis. 156, 105405.
Murata, M.M., Kong, X., Moncada, E., Chen, Y., Imamura, H., Wang, P., Berns, M.W., Yokomori, K., Digman, M.A., 2019. NAD+ consumption by PARP1 in response to DNA damage triggers metabolic shift critical for damaged cell survival. Mol. Biol. Cell 30, 2584–2597.
Nagley, P., Higgins, G.C., Atkin, J.D., Beart, P.M., 2010. Multifaceted deaths orchestrated by mitochondria in neurones. Biochim. Biophys. Acta Mol. basis Dis. 1802, 167–185.
Nathans, J., Thomas, D., Hogness, D.S., 1986. Molecular genetics of human color vision : the genes encoding blue, green and red pigments. Science (80) 232, 193–202.
Norrie, J.L., Lupo, M.S., Xu, B., Al Diri, I., Valentine, M., Putnam, D., Griffiths, L., Zhang, J., Johnson, D., Easton, J., et al., 2019. Nucleome dynamics during retinal development. Neuron 104, 512–528.e11.
Peng, G.H., Ahmad, O., Ahmad, F., Liu, J., Chen, S., 2005. The photoreceptor-specific nuclear receptor Nr2e3 interacts with Crx and exerts opposing effects on the transcription of rod versus cone genes. Hum. Mol. Genet. 14, 747–764.
Peng, Y.-R., Shekhar, K., Yan, W., Herrmann, D., Sappington, A., Bryman, G.S., van Zyl, T., Do, M.T.H., Regev, A., Sanes, J.R., 2019. Molecular classification andcomparative taxonomics offovealandperipheralcellsinprimateretina. Cell 176, 1222.
Persiconi, I., Cosmi, F., Guadagno, N.A., Lupo, G., De Stefano, M.E., 2020. Dystrophin is required for the proper timing in retinal Histogenesis: A thorough investigation on the mdx mouse model of Duchenne muscular dystrophy. Front. Neurosci. 14, 760.
Pfeiffer, R.L., Marc, R.E., Jones, B.W., 2020. Persistent remodeling and neurodegeneration in late-stage retinal degeneration. Prog. Retin. Eye Res. 74, 100771.
Ripamonti, C., Aboshiha, J., Henning, G.B., Sergouniotis, P.I., Michaelides, M., Moore, A. T., Webster, A.R., Stockman, A., 2014. Vision in observers with enhanced S-cone syndrome: an excess of S-cones but connected mainly to conventional S-cone pathways. Invest. Ophthalmol. Vis. Sci. 55, 963–976.
Roesch, K., Jadhav, A.P., Trimarchi, J.M., Stadler, M.B., Roska, B., Sun, B.B., Cepko, C.L., 2008. The transcriptome of retinal Müller glial cells. J. Comp. Neurol. 509, 225.
Ruether, K., Feigenspan, A., Pirngruber, J., Leitges, M., Baehr, W., Strauss, O., 2010. PKCα is essential for the proper activation and termination of rod bipolar cell response. Invest. Ophthalmol. Vis. Sci. 51, 6051.
Sakaguchi, H., Miyagi, M., Darrow, R.M., Crabb, J.S., Hollyfield, J.G., Organisciak, D.T., Crabb, J.W., 2003. Intense light exposure changes the crystallin content in retina. Exp. Eye Res. 76, 131–133.
Samson, A.L., Zhang, Y., Geoghegan, N.D., Gavin, X.J., Davies, K.A., Mlodzianoski, M.J., Whitehead, L.W., Frank, D., Garnish, S.E., Fitzgibbon, C., 2020. et al. MLKL Trafficking and Accumulation at the Plasma Membrane Control the Kinetics and Threshold for Necroptosis.
Schnapf, J.L., Kraft, T.W., Baylor, D.A., 1987. Spectral sensitivity of human cone photo receptors. Nature 325, 439–441.
Schorderet, D.F., Escher, P., 2009. NR2E3 mutations in enhanced S-cone sensitivity syndrome (ESCS), Goldmann-Favre syndrome (GFS), clumped pigmentary retinal degeneration (CPRD), and retinitis pigmentosa (RP). Hum. Mutat. 30, 1475–1485.
Shekhar, K., Lapan, S.W., Whitney, I.E., Tran, N.M., Macosko, E.Z., Kowalczyk, M., Adiconis, X., Levin, J.Z., Nemesh, J., Goldman, M., et al., 2016. Comprehensive classification of retinal bipolar neurons by single-cell transcriptomics. Cell 166, 1308–1323.e30.
Stuart, T., Butler, A., Hoffman, P., Hafemeister, C., Papalexi, E., Mauck, W.M., Hao, Y., Stoeckius, M., Smibert, P., Satija, R., 2019. Comprehensive integration of single-cell data. Cell 177, 1888–1902.e21.
Sun, C., Zhang, X., Ruzycki, P.A., Chen, S., 2022. Essential functions of MLL1 and MLL2 in retinal development and cone cell maintenance. Front. Cell Dev. Biol. 10.
Swaroop, A., Kim, D., Forrest, D., 2010. Transcriptional regulation of photoreceptor development and homeostasis in the mammalian retina. Nat. Rev. Neurosci. 11, 563–576.
Tan, M.H.E., Zhou, X.E., Soon, F.F., Li, X., Li, J., Yong, E.L., Melcher, K., Xu, H.E., 2013. The crystal structure of the orphan nuclear receptor NR2E3/PNR ligand binding domain reveals a dimeric auto-repressed conformation. PLoS One 8, 1–13.
Templeton, J.P., Di Wang, X., Freeman, N.E., Ma, Z., Lu, A., Hejtmancik, F., Geisert, E.E., 2013. A Crystallin gene network in the mouse retina. Exp. Eye Res. 116, 129.
Toulis, V., Garanto, A., Marfany, G., 2016. Combining zebrafish and mouse models to test the function of deubiquitinating enzyme (dubs) genes in development: Role of USP45 in the retina. In: Matthiesen, R. (Ed.), Proteostasis: Methods and Protocols. New York, NY, Springer New York, pp. 85–101.
Trimarchi, J.M., Stadler, M.B., Cepko, C.L., 2008. Individual retinal progenitor cells display extensive heterogeneity of gene expression. PLoS One 3, e1588.
Tsukamoto, Y., Morigiwa, K., Ueda, M., Sterling, P., 2001. Microcircuits for night vision in mouse retina. J. Neurosci. 21, 8616–8623.
Uren, P.J., Lee, J.T., Mehdi Doroudchi, M., Smith, A.D., Horsager, A., 2014. A profile of transcriptomic changes in the rd10 mouse model of retinitis pigmentosa. Mol. Vis. 20, 1612–1628.
Vanden Berghe, T., Linkermann, A., Jouan-Lanhouet, S., Walczak, H., Vandenabeele, P., 2014. Regulated necrosis: the expanding network of non-apoptotic cell death pathways. Nat. Rev. Mol. Cell Biol. 152 (15), 135–147.
Venturini, G., Kokona, D., Steiner, B.L., Bulla, E.G., Jovanovic, J., Zinkernagel, M.S., Escher, P., 2021. In vivo analysis of onset and progression of retinal degeneration in the Nr2e3rd7/rd7 mouse model of enhanced S-cone sensitivity syndrome. Sci. Report. 11, 1–14.
Woods, S.M., Mountjoy, E., Muir, D., Ross, S.E., Atan, D., 2018. A comparative analysis of rod bipolar cell transcriptomes identifies novel genes implicated in night vision. Sci. Report. 8, 1–15.
Wunderlich, K.A., Tanimoto, N., Grosche, A., Zrenner, E., Pekny, M., Reichenbach, A., Seeliger, M.W., Pannicke, T., Perez, M.T., 2015. Retinal functional alterations in mice lacking intermediate filament proteins glial fibrillary acidic protein and vimentin. FASEB J. 29, 4815–4828.
Xie, S., Han, S., Qu, Z., Liu, F., Li, J., Yu, S., Reilly, J., Tu, J., Liu, X., Lu, Z., et al., 2019. Knockout of Nr2e3 prevents rod photoreceptor differentiation and leads to selective L−/M-cone photoreceptor degeneration in zebrafish. Biochim. Biophys. Acta Mol. basis Dis. 1865, 1273–1283.
Yan, J., Chen, Y., Zhu, Y., Paquet-Durand, F., 2021. Programmed non-apoptotic cell death in hereditary retinal degeneration: crosstalk between cGMP-dependent pathways and PARthanatos? Int. J. Mol. Sci. 22, 10567.
Yoon, S., Kovalenko, A., Bogdanov, K., Wallach, D., 2017. MLKL, the protein that mediates necroptosis, also regulates endosomal trafficking and extracellular vesicle generation. Immunity 47, 51–65.e7.
Yoshimura, N., Kikuchi, T., Kuroiwa, S., Gaun, S., 2003. Differential temporal and spatial expression of immediate early genes in retinal neurons after ischemia-reperfusion injury. Invest. Ophthalmol. Vis. Sci. 44, 2211–2220.
Young, M.D., Behjati, S., 2020. SoupX removes ambient RNA contamination from droplet-based single-cell RNA sequencing data. Gigascience 9.
Zheng, G.X.Y., Terry, J.M., Belgrader, P., Ryvkin, P., Bent, Z.W., Wilson, R., Ziraldo, S.B., Wheeler, T.D., McDermott, G.P., Zhu, J., et al., 2017. Massively parallel digital transcriptional profiling of single cells. Nat. Commun. 8.